ChemPubSoc Europe

DOI: 10.1002/open.201900344

Open Access ChemistryOPEN Full Paper

Synthesis, Evaluation and Proposed Binding Pose of Substituted Spiro-Oxindole Dihydroquinazolinones as IRAP Inhibitors

Karin Engen,[a] Sudarsana Reddy Vanga,[b] Thomas Lundbäck,[c, d] Faith Agalo,[a] Vivek Konda,[a] Annika Jenmalm Jensen,[c] Johan Åqvist,[b] Hugo Gutiérrez-de-Terán,[e] Mathias Hallberg,[f] Mats Larhed,[g] and Ulrika Rosenström*[a]

Insulin-regulated aminopeptidase (IRAP) is a new potential macromolecular target for drugs aimed for treatment of cognitive disorders. Inhibition of IRAP by angiotensin IV (Ang IV) improves the memory and learning in rats. The majority of the known IRAP inhibitors are peptidic in character and suffer from poor pharmacokinetic properties. Herein, we present a series of small non-peptide IRAP inhibitors derived from a spiro-oxindole dihydroquinazolinone screening hit (pIC_{50} 5.8). The compounds were synthesized either by a simple microwave (MW)-promoted three-component reaction, or by a two-step one-pot procedure. For decoration of the oxindole ring system, rapid MW-assisted Suzuki-Miyaura cross-couplings (1 min) were performed. A small improvement of potency (pIC_{50} 6.6 for the most potent compound) and an increased solubility could be achieved. As deduced from computational modelling and MD simulations it is proposed that the *S*-configuration of the spiro-oxindole dihydroquinazolinones accounts for the inhibition of IRAP.

1. Introduction

Insulin-regulated aminopeptidase (IRAP, oxytocinase, EC 3.4.11.3) is an enzyme abundantly expressed in areas of the brain associated with cognition, including amygdala, hippocampus and cerebral cortex. Interference with the aminopeptidase activity, such as after administration of the endogenous hexapeptide angiotensin IV (Ang IV), has demonstrated that cognitive enhancement in experimental models can be accomplished.[1–4] Mechanistically IRAP has the unique ability to cleave the *N*-terminal peptide bonds of macrocyclic peptidic regulators of cognition, such as oxytocin and vasopressin.[5–8]

The interest in IRAP as a potential target for treatment of cognitive disorders has grown during the last decade. However, IRAP also mediates several important physiological and pathological activities not only those associated to cognition. It has also an impact on parameters related to immunology, *i.e.* antigen processing and trafficking of T-cells receptors; glucose metabolism, *i.e.* trafficking of glucose transporters; and fibrosis, *i.e.* regulation of fibrotic responses in heart and kidney.[9–15] Hence, efficient inhibitors of IRAP could serve as a potential new class of cognitive enhancers in the future, but in addition conceivably, also act as agents useful for *e.g.* regulation of immune responses. Highly potent peptidic and pseudo-peptidic IRAP inhibitors with selectivity for IRAP, as opposed to other aminopeptidases, have been identified.[16–20] Our group synthesized both linear and constrained Ang IV analogues[21–23] and macrocycles mimicking the *N*-terminal of oxytocin and obtained a series of inhibitors with high potency and stability.[24,25] One of the compounds, **HA08** (see Figure 1), was recently proven to alter dendritic spine density in rat hippocampal primary cultures.[26] However, **HA08** and structurally related analogues are still peptidic in character and are foreseen to suffer from

[a] K. Engen, Dr. F. Agalo, V. Konda, Dr. U. Rosenström
Department of Medicinal Chemistry
Uppsala University
SE-751 23 Uppsala, SWEDEN
E-mail: ulrika.rosenstrom@ilk.uu.se
[b] Dr. S. R. Vanga, Prof. J. Åqvist
Department of Cell and Molecular Biology
Uppsala University
SE-751 23 Uppsala, SWEDEN
[c] Dr. T. Lundbäck, Dr. A. J. Jensen
Chemical Biology Consortium Sweden, Science for Life Laboratory, Department of Medical Biochemistry and Biophysics
Karolinska Institutet
SE-171 65 Solna, SWEDEN
[d] Dr. T. Lundbäck
Mechanistic Biology & Profiling, Discovery Sciences, R&D
AstraZeneca
SE-431 83 Göteborg, SWEDEN
[e] Dr. H. Gutiérrez-de-Terán
Science for Life Laboratory, Department of Cell and Molecular Biology
Uppsala University
SE-751 23 Uppsala, SWEDEN
[f] Prof. Dr. M. Hallberg
The Beijer Laboratory, Department of Pharmaceutical Biosciences
Uppsala University
SE-751 23 Uppsala, SWEDEN
[g] Prof. Dr. M. Larhed
Science for Life Laboratory, Department of Medicinal Chemistry
Uppsala University
SE-751 23 Uppsala, SWEDEN

Supporting information for this article is available on the WWW under https://doi.org/10.1002/open.201900344

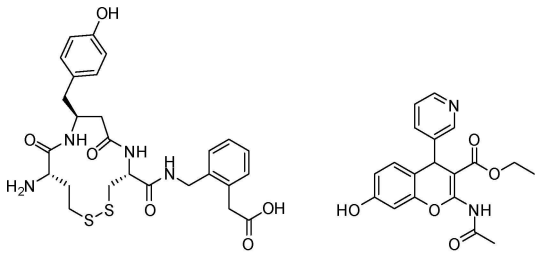

Figure 1. Two examples of known IRAP inhibitors.

low bioavailability and a limited ability to pass the blood-brain-barrier. The first published drug-like class of IRAP inhibitors, encompassing a benzopyran scaffold (*e.g.* **HFI-419**), has been reported to exhibit a dose-dependent improvement of visual recognition task in rats. Administration in lateral ventricles also improved spatial working memory.[27] Furthermore, it was recently proposed that these IRAP inhibitors facilitate memory by increasing hippocampal dendritic spine density via a GLUT4-mediated mechanism.[28] Altogether, these benzopyran-based molecules represent the first generation of non-peptidic IRAP inhibitors that elicit effects in *in vivo* experimental models. Unfortunately, this class of inhibitors seems to be associated with a relatively short half-life and high plasma clearance.[29]

The promising *in vivo* results encouraged us to commence a screening campaign applying an IRAP activity assay based on natural expression of the target in Chinese Hamster Ovary (CHO) cells to identify novel drug-like IRAP inhibitors. A compound library of approximately 10 500 compounds was screened and a limited number of hit families were identified.[30] The basic structure activity relationship (SAR) of an arylsulfonamide-based class of inhibitors from this screen was recently reported, and we could also demonstrate that these compounds can increase the number of mushroom-shaped dendritic spines, a morphology associated with memory enhancement.[31–33]

Herein, we report the synthesis and initial SAR of a new class of small-molecule IRAP inhibitors, comprising a spiro-oxindole dihydroquinazolinone scaffold, originating from a hit compound (**1**) exhibiting a pIC_{50} value of 5.8.[30] Compound **1** is relatively lipophilic with a measured logD of 3.4 and suffers from poor solubility and metabolic stability (Tables 1 and 2). Our aims in this study were to gain a better understanding of the SAR around this scaffold, define the mechanism of IRAP inhibition and use this knowledge to improve the properties of compound **1**.

2. Results and Discussion

Two and three-component reactions of structurally similar compounds have been published, typically requiring reflux for several hours.[34–39] We aimed to improve the synthetic procedures for this type of scaffold and have previously demonstrated that compound **1** can be synthesized alongside a series of analogs in a smooth and scalable way using microwave (MW) heated continuous flow synthesis (**1**–**3**, **23**, **26**–**29**, **31**).[40,41] Here we show that these spiro-compounds can be obtained utilizing MW heated batch chemistry in a rapid and simple way. By mixing isatoic anhydride, the appropriate aniline and the appropriate isatin in acetic acid and heat the reaction in a sealed vial using MW irradiation for 10 min, the desired compounds (**4**–**7**, **9**, **24**–**25**) could be obtained in moderate to excellent yields (53–93%, Scheme 1). By utilizing this method, compounds with variations in position 1, 5 and 7 could be investigated (see Table 1 for nomenclature). Evaluation of the

Table 1. Evaluation of compounds **1**–**24** as IRAP inhibitors.

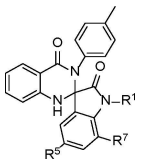

Cmpd	R^1	R^5	R^7	pIC_{50} [a]
1	H_3C	Br	H	5.8 ± 0.2 (21)[b] 4.8 ± 0.02 (2)[c] Inactive (2)[d]
2	H_3C	H	H	4.0 ± 0.4 (4)[b]
3	H_3C	H	Br	Inactive (3)[b]
4	H_3C	F	H	4.9 ± 0.03 (3)[b]
5	H_3C	Cl	H	5.7 ± 0.03 (3)[b]
6	H_3C	I	H	6.0 ± 0.06 (3)[b]
7	H_3C	O_2N	H	5.8 ± 0.08 (5)[b] 4.5 ± 0.01 (2)[c] Inactive (2)[d]
8	H_3C	H_2N	H	< 3.9 (3)[b]
9	H_3C	H_3CO	H	4.8 ± 0.3 (3)[b]
10	H_3C	H_3C	H	4.8 ± 0.2 (3)[b]
11	H_3C	4-fluorophenyl	H	< 3.9 (3)[b]
12	H_3C	4-phenoxyphenyl	H	Inactive (3)[b]
13	H_3C	3-acetamidyl	H	Inactive (4)[b]
14	H_3C	4-cyanophenyl	H	Inactive (3)[b]
15	H_3C	2-ethylphenyl	H	< 3.9 (3)[b]
16	H_3C	2-methoxyphenyl	H	< 3.9 (3)[b]
17	H_3C	*p*-tolyl	H	Inactive (3)[b]
18	H_3C	4-pyridinyl	H	4.2 ± 0.4 (4)[b]
19	H_3C	8-quinolinyl	H	4.1 ± 0.4 (3)[b]
20	H_3C	2-thiophenyl	H	< 3.9 (3)[b]
21	H_3C		H	Inactive (4)[b]
22	H_3C	(*E*)-styryl	H	Inactive (3)[b]
23	H	Br	H	4.6 ± 0.3 (4)[b]
24	H	H	H	< 3.9 (3)[b]

[a] Reported pIC_{50} values represent the mean ± standard deviation of best-fit values (the number of independent test occasions is provided within brackets). No values below 3.9 are reported as this was the highest compound concentration tested. [b] Evaluated on IRAP from CHO cells. [c] Evaluated on human membrane bound IRAP overexpressed in HEK293 cells. [d] Evaluated on human aminopeptidase N overexpressed in HEK293 cells.

Table 2. Evaluation of selected compounds regarding lipophilicity, solubility, *in vitro* metabolic stability and plasma protein binding.

Cmpd	$LogD_{7.4}$	Sol.[a]	HLM Cl_{int}[b]	HLM $t_{1/2}$	Rat hep. Cl_{int}[c]	Rat hep. $t_{1/2}$	PPB[d]	Plasma stab[e]
1	3.4±0.1	0.2–1.4[f]	>300[h]	<2.3[h]	135±11	5.2±0.4	4.3±0.5	106±11
7	2.7±0.1	1.8±0.3	>300[h]	<2.3[h]	114±4	6.1±0.2	9.8±2	100±5
15	4.9±0.1	0.2±0.1[g]	>300[h]	<2.3[h]	>300[h]	<2.3[g,h]	0.25–3.2	102±25
32_1	3.7±0.1	0.3–3.5[f]	>300[h]	<2.3[h]	>300[g,h]	<2.3[g,h]	1.9±0.5	101±7
32_2	3.8±0.2	0.1–1.3[f]	>300[h]	<2.3[h]	168±20[h]	4.2±0.5[h]	1.5±0.3	99±3
36	2.6±0.1	20±1.2	>300[h]	<2.3[h]	84±14	8.5±1.6	5.5±0.4	97±15
37	3.0±0.1	4–16[f]	>300[h]	<2.3[h]	132±39[h]	5.5±1.4[h]	4.1±0.8	98±3
38	3.7±0.1	2.4–7.5[f]	>300[h]	<2.3[h]	248±5[h]	2.8±0.06[h]	1.9±0.4	105±7
39	2.4±0.01	58±16	>300[h]	<2.3[h]	91±8	7.6±0.6	14±0.6	99±1
40	1.6±0.1	814±63	81±10	8.6±1.0[g]	136±22	5.2±0.9	40±4	95±2

All data are reported as the average and standard deviation from three independent test occasions. [a] Dried DMSO solubility in aqueous phosphate buffer (PBS) at pH 7.4; μM. [b] Human liver microsome intrinsic clearance; μL/min/mg. [c] Rat hepatocytes intrinsic clearance; μL/min/10^6 cells. [d] Human protein plasma binding; % free. [e] Human plasma stability; % compound remaining after 18 h incubation. [f] High-throughput solubility assays are associated with large variability, especially below 10 μM range. When the standard deviation is higher than half the mean value, the entire range is given. [g] An outlier value was observed with higher solubility amongst the three replicates. The higher value was removed. Also in the metabolic assays when an outlier with lower clearance or longer half-life was detected among the three replicates, this value was removed. [h] A higher uncertainty is associated with these values as compound dilutions resulted in non-linear responses.

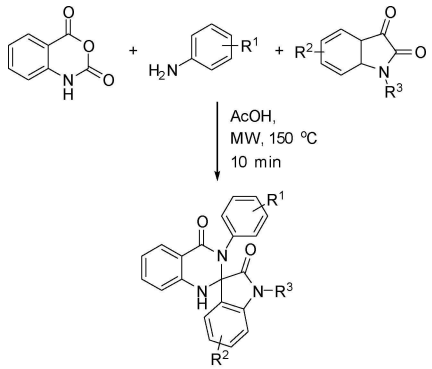

Scheme 1. Improved batch synthesis of the spiro-structure employing aryl-amines.

synthesized compounds revealed that a substituent in the 5-position of the oxindole moiety was crucial for inhibition. Removal of the bromine (**2**) resulted in loss of activity and displacement to the 7-position (**3**) resulted in an inactive compound.

Exchange of the bromine for the other halogens fluorine (**4**), chlorine (**5**) and iodine (**6**) resulted in slightly increased activity from fluorine to iodine. Substitution of the bromine with a nitro group (**7**) retained activity, whilst reduction to the amine (**8**) reduced the activity dramatically. A methoxy (**9**) or methyl-group (**10**) instead of the original bromine also resulted in loss of activity by tenfold.

Since the screen was performed on IRAP derived from CHO-cells, we also wanted to confirm inhibitory activity on the human orthologue (hIRAP) as well as to investigate selectivity against the closely related aminopeptidase N (APN). The hit compound **1** and the equipotent analog **7** were both evaluated in this respect (Table 1). Both compounds lost approximately 10 to 15-fold activity on hIRAP compared to IRAP from CHO-cells, meaning the potency approached a concentration where visual precipitation was observed (>50 μM). Sequence analysis revealed that the few differences between the two orthologue IRAP enzymes (sequence ID=88%, data not shown) are not located in the binding site residues. As described below, a key driver in the further optimization has thus been to improve on compound solubility to get a better separation between observed potencies and solubilities to improve on these comparisons. Both compounds were shown to be completely inactive on the closely related APN under identical assay conditions, *i.e.* demonstrating selectivity for IRAP (Table 1).

As the previous results indicated that an electron-withdrawing and/or lipophilic substituent in the 5-position was beneficial for inhibition, we performed Suzuki-Miyaura cross couplings on **1** to incorporate aryl and vinyl groups (**11**–**22**, Scheme 2), in order to further explore the SAR of lipophilic substituents at this position. The reaction conditions were optimized in order to increase reaction speed and reduce dehalogenation and hydrolysis of the aminal part. Different Pd-catalysts, bases, solvent systems, temperatures and equivalents of boronic acid were investigated. It could be concluded that dehalogenation was affected by solvent and base, but not by concentration, temperature or Pd-source.

Minimization of the water content and slight excess of base was necessary to avoid hydrolysis.[41] The reaction optimization resulted in a swift and simple MW-procedure to obtain the desired compounds in only a few minutes (Scheme 2).

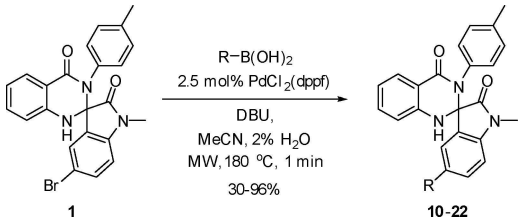

Scheme 2. Suzuki-Miyaura cross couplings to introduce different aryl, heteroaryl and vinyl substituents.

Introduction of substituted aryls (**11**–**17**), heteroaryls (**18**–**20**) or vinyl groups (**21**–**22**) rendered inactive or compounds with poor activity compared to **1**. In summary, introduction of these kind of lipophilic substituents in the 5-position seemed to be detrimental for activity, indicating that the electron-withdrawing properties of previous substituents (**1**, **4**–**10**) rendered the active compounds. Regarding the *N*-substituent of the oxindole moiety, removal of the methyl group (**23**) decreased the activity 30-fold, and removal of both the methyl and the bromine (**24**) decreased the activity even more. Since the compounds did not show any improvement in potency on IRAP from CHO-cells, none of the compounds were evaluated on the human orthologue.

Since no potency or DMPK improvements (Table 2) were observed when substituting the oxindole part of **1**, we next investigated the *p*-tolyl moiety (Table 3). Removal of the entire moiety as in **25** resulted in a small drop of activity. Removal of the methyl group (**26**) or exchange to a triflouromethyl (**27**) also gave a slight activity loss. Substitution with a larger *tert*-butyl group (**28**) or iodine (**29**) provided compounds with the same activity as the hit compound (**1**). Similar activities were also observed when introducing a benzyloxy substituent (**30**) or an oxazole ring in the *meta* position (**31**). When we incorporated a carbon linker between the scaffold and the aryl group, hence used aliphatic amines, we had to modify the reaction conditions for the synthesis. Instead of using acetic acid as both solvent and catalyst, we used ethanol as solvent applying 5% AcOH as catalyst to obtain the intermediate A when reacting isatoic anhydride with the appropriate amine (Scheme 3). A quick solvent evaporation followed by dissolution in EtOH and this time adding 1% TFA as catalyst to perform the final MW-promoted ring closure reaction gave compounds **30**, **32**–**41** in 53–82% yield over two steps (Scheme 3). Introduction of a one-carbon spacer between the scaffold and the aromatic ring (**32**) resulted in the first compound with higher inhibitory capacity than the hit compound (Table 3). However, also this compound lost activity on human IRAP, *i.e.* in agreement with observations made for **1** and **7**. Despite the reduced potency on human IRAP, **32** was separated into the pure enantiomers by chiral supercritical fluid chromatography (SFC) and these were evaluated for their inhibitory capacities. The most active enantiomer (**32_1**) displayed a pIC_{50}-value of 6.7, whereas the other enantiomer (**32_2**) was more than two orders of magnitude less potent (4.1). No substantial differences between the enantiomers were observed regarding solubility, *in vitro* metabolic stability or plasma protein binding (Table 2). Additional SAR-investigation in this position revealed that elongation of the linker with one additional carbon (**33**) reduced the activity somewhat, but still rendered a better inhibitor than the parent compound. A saturated cyclohexyl (**34**) also moderately increased the inhibition compared to **1**. Substitution with heteroaryls such as 2-pyridyl (**35**), 3-pyridyl (**36**) or furyl (**37**), in an attempt to increase the solubility compared to **32**, unfortunately provided compounds with lower potency. Moreover, despite being more polar (see Table 2), these compounds also lost activity on human IRAP. Introduction of a saturated carbon chain (**38**) furnished the most active compound in this series so far. Again,

Table 3. Evaluation of compounds **25**–**41** as IRAP-inhibitors.

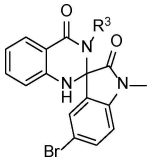

Cmpd	R^3	pIC_{50}[a]
25	H	5.2 ± 0.2 (3)[b]
26	phenyl	5.2 ± 0.4 (3)[b]
27	4-(trifluoromethyl)phenyl	5.3 ± 0.1 (3)[b]
28	4-(*tert*-butyl)phenyl	5.7 ± 0.3 (3)[b]
29	4-iodophenyl	5.5 ± 0.2 (3)[b]
30	4-(benzyloxy)phenyl	5.5 ± 0.3 (3)[b]
31	3-(oxazol-5-yl)phenyl	5.7 ± 0.3 (3)[b]
32	CH_2Ph	6.4 ± 0.2 (5)[b] 5.3 ± 0.01 (2)[c] Inactive (2)[d]
32_1	1st eluted enantiomer	6.7 ± 0.05 (4)[b]
32_2	2nd eluted enantiomer	4.1 ± 0.2 (4)[b]
33	CH_2CH_2Ph	6.2 ± 0.07 (3)[b]
34	CH_2-cyclohexyl	6.2 ± 0.1 (3)[b]
35	CH_2-(2-pyridinyl)	5.2 ± 0.2 (3)[b]
36	CH_2-(3-pyridinyl)	5.7 ± 0.06 (3)[b] 4.5 ± 0.05 (2)[c] Inactive (1)[d]
37	CH_2-(2-furanyl)	6.2 ± 0.07 (3)[b] 4.9 ± 0.1 (2)[c] Inactive (1)[d]
38	$CH_2CH_2CH_2CH_3$	6.6 ± 0.05 (3)[b]
39	$CH_2CH_2OCH_3$	5.5 ± 0.02 (3)[b] 4.3 ± 0.07 (2)[c] Inactive (1)[d]
40	$CH_2CH_2N(CH_3)_2$	5.6 ± 0.08 (3)[b] 4.4 ± 0.04 (2)[c] Inactive (1)[d]
41	$CH_2CH_2CH_2N(CH_3)_2$	4.7 ± 0.1 (3)[b]

[a] pIC_{50} = negative log of the IC_{50} in molar. Values represent the mean ± standard deviation of best-fit values (the number of independent test occasions is provided within brackets). No values below 3.9 are reported as this was the highest compound concentration tested. [b] Evaluated on IRAP from Chinese hamster ovary cells. [c] Evaluated on human membrane bound IRAP overexpressed in HEK293 cells. [d] Evaluated on human aminopeptidase N overexpressed in HEK293 cells.

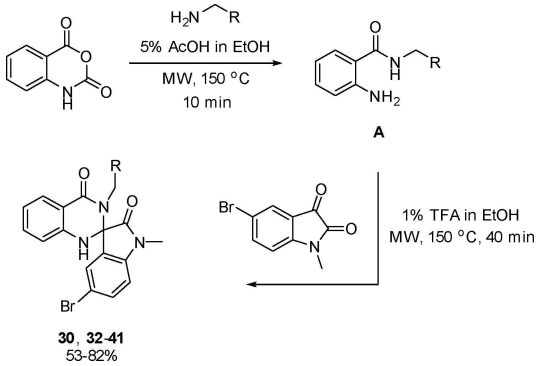

Scheme 3. Modified two step synthesis of the spiro-structure employing aliphatic amines.

since we had seen that the compounds lost activity on human IRAP, we next tried to synthesize more soluble derivatives. However, introduction of heteroatoms in the chains (**39**–**41**) decreased the inhibition compared to **38**, indicating that a lipophilic substituent in this part of the molecule is favorable but not necessary. Despite improved solubility (Table 2), these compounds lost activity on human IRAP, while retaining selectivity for IRAP versus APN. It should be emphasized that compound **40** is equipotent with the hit compound (**1**), but shows considerably better solubility, indicating that it is possible to improve this property while maintaining activity. Unfortunately, all compounds synthesized in order to improve solubility still suffered from poor *in vitro* metabolic stability properties in both human liver microsomes and rat hepatocytes. The plasma protein binding is an issue with compound **1** and most of the tested compounds, with the exception of compound **40** which has a large free fraction.

We were interested in better understanding the mode of action of these compounds and whether the observed SAR could be rationalized in terms of their interaction with IRAP. This prompted us to perform docking studies of selected compounds in an attempt to discover their putative binding site. Ligands **1**, **3**, **12**, **24**, **32**, **38** and **40** were selected for docking studies on the basis of their measured potencies in the enzymatic assay. An initial analysis of the protein surface area, based on the available IRAP crystal structures, (open and closed conformations), allowed the identification of three potential sites for small molecule binding, herein referred to as H (Histidine-cluster), A (allosteric site), and Z (Zinc-site), depicted in Supporting Information Figure S1.

In the open conformation of IRAP (PDB ID: 4PJ6), independent docking of the two stereoisomers on the H- and A-sites did not yield any conserved binding mode that was compatible with the SAR extracted from Tables 1 and 3. Conversely, all the ligands in their *S* configuration, with the only exception of compound **12**, found a conserved binding mode on the Z-site (see Supporting Information Figure S1). While being in the vicinity of the Zn^{2+}, the ligand is not coordinating the ion, having the *N*-Me at 4 Å distance to the ion. In this pose the oxindole moiety makes a hydrogen bond to Tyr549 while the bromine is coordinated to Arg439. The second ring is making a π-π stacking interaction with Phe544, which is only possible when considering the *S* stereoisomer. Similar docking exploration was performed on the closed conformation of IRAP crystal structure (PDB ID: 5MJ6).[42] The results from the docking in this "closed" conformation of IRAP did not show any conserved binding pose that could explain the SAR of the series.

To check the stability of this binding mode, obtained in the "open" conformation of IRAP, we performed MD simulations of the complex with ligand **38**, one of the most potent compounds in the series. The average root-mean-square deviation (RMSD) along all replica simulations is 0.44 ± 0.01 Å for protein backbone and 2.26 ± 0.5 Å for the ligand. This indeed results in a refined position for the ligand, which is shown in Figure 2. While this refined pose is mostly consistent with the initial docking, the main difference is located in the translation of the ligand by approximately additional 1.5 Å away from Zn^{2+}, allowing a water molecule to insert in between Tyr549 and the oxygen from the oxindole (Figure 2). As the zinc ion is a critical component of substrate recognition and processing during the catalytic cycle, we wondered if the space between the ligand and the Zn^{2+} ion could simultaneously accommodate the small L-Leu-*p*NA substrate used in our assays, and whether such simultaneous binding would retain discrimination between *S* and *R* stereoisomers. Superposition of the IRAP-substrate complex with the IRAP-**38** equilibrated pose (Figure 2b) shows how the substrate is predicted to bind, placing the Leucine and *para*-nitrophenyl groups in equivalent

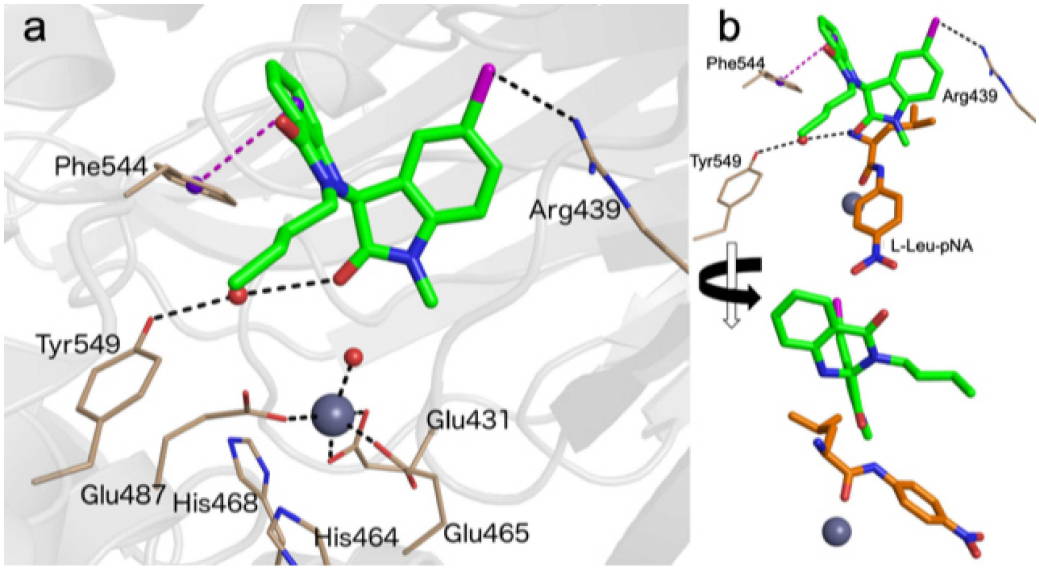

Figure 2. a) Binding mode of ligand **38** (green sticks) in IRAP obtained from a representative snapshot from the MD simulation. b) The same snapshot, with the superposition of substrate L-Leu-*p*NA (orange sticks) as docked to IRAP, in two different points of view. Zn^{2+} and water molecules are shown as grey and red spheres, respectively, and bromine atoms are represented in magenta. Key residues are shown in wheat colour sticks

positions to the Val[1] and Tyr[2] sidechains of Ang IV.[26] As described below this model of simultaneous binding of inhibitor **38** and substrate L-Leu-*p*NA prompted further experimental verification of the mechanism of action, *i.e.* to what extent compound binding is competitive, non-competitive or uncompetitive with substrate binding.

We next examined whether the proposed binding pose could also explain the SAR observed for this series. The orientation of the 5-position of the oxindole moiety, *i.e.* the one holding the bromine in the original hit compound **1**, is in line with the high propensity observed for the interactions of halogens with arginine,[43] explaining why the replacement of the halogenated or electron withdrawing groups in active compounds **4**–**7** by either aryl (**11**–**17**), heteroaryl (**18**–**20**) or vinyl groups (**21**–**22**) rendered inactive or weakly active compounds (Table 1). This is also in line with the inability of compound **12**, carrying the bulkiest substituent at this position, to find this binding mode. Encouragingly, the ranking of the compounds based on their pIC_{50} values is reproduced by the tendency of the scoring function, with the exception of ligand **32** (Supporting Information Table 1).

In order to complement the docking studies and to better understand whether the substrate can be simultaneously accommodated in the active site, we performed a set of additional experiments. First, enzyme kinetics experiments revealed that compound **32** act as an uncompetitive inhibitor to L-Leu-*p*NA (Figure 3), suggesting it does not bind at a mutually exclusive binding site, *i.e.* in the immediate vicinity of the catalytic Zn^{2+} ion. This is in contrast to previously published IRAP inhibitors. Although these data are in line with the simultaneous binding model as presented in Figure 2b, the uncommon observation of an uncompetitive inhibition pattern prompted us to look back at previously established data in our labs as to the reversible nature of the interaction. We have previously reported data from jump-dilution experiments with compound **1**,[30] demonstrating a fully reversible behavior. To further corroborate this finding, we had also performed inhibition experiments in which the incubation time for the enzymatic reaction was allowed to extend beyond completion. Such over incubation is expected to result in a significant loss of sensitivity to reversible inhibitors,[44] and indeed we observed a right-shifting of the concentration responses over time (Supporting Information Figure S2). Taken together, these data verify the inability of **1** to irreversibly inactivate IRAP and demonstrates the ability of a representative compound to bind simultaneously as the substrate to IRAP.

The tested ligands (**1**, **7**, **32**, **36**–**37**, and **39**–**40**) demonstrated specificity for IRAP over human APN as reported in Tables 1 and 3. Accordingly, attempts to dock these ligands in the corresponding site in APN (PDB ID: 4FYQ) did not yield any binding poses, as it also occurred with docking on the closed conformation of IRAP. The specificity of the binding orientation discussed above for the IRAP-open conformation is illustrated by superposition of the obtained complex in this structure, with the APN and IRAP-closed crystal structures (Figure 4). The figure illustrates how the selectivity for IRAP-open conformation might come from the GAMEN loop, which in the IRAP-closed

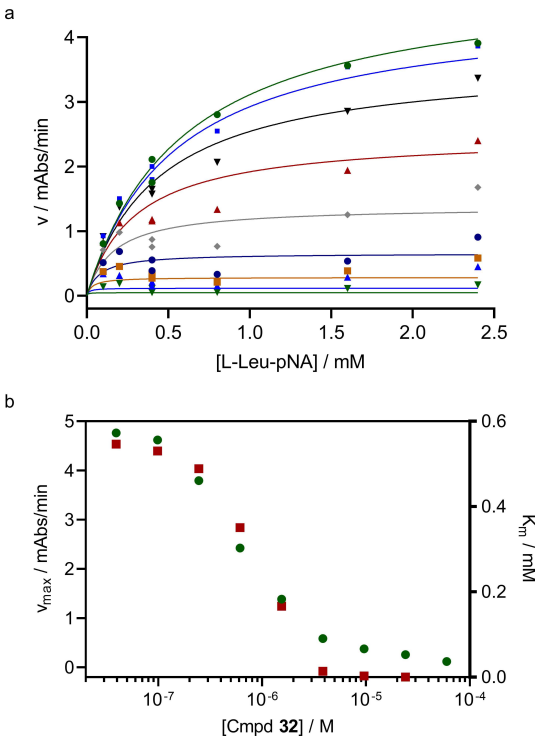

Figure 3. a) IRAP reaction rates as a function of substrate concentration for compound **32** at concentrations between 39 nM and 150 μM. The solid lines represent the best fit to a model for uncompetitive inhibition, resulting in a K_m value of 0.67 ± 0.07 mM, a V_{max} of 5.3 ± 0.3 mAbs/min and a K_i value of 0.54 ± 0.06 μM. b) Best-fit K_m (■) and V_{max} (●) values when the data were instead fitted to a Michaelis-Menten model for each compound concentration with no assumption of the inhibition mode.

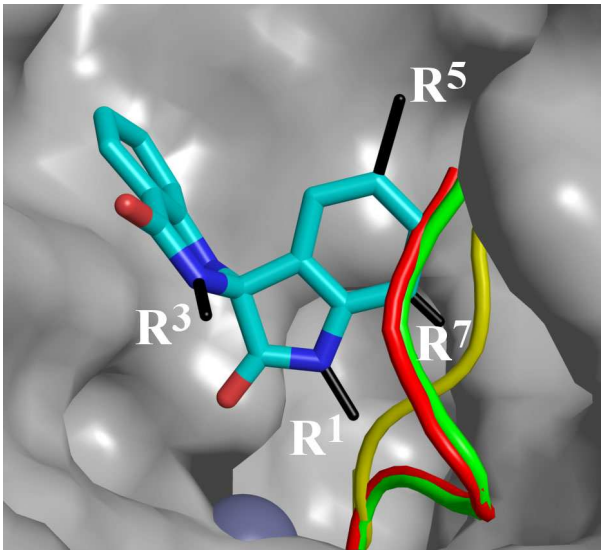

Figure 4. Binding mode of ligand core (cyan color sticks), in IRAP superimposed with APN and IRAP-closed conformation. The GAMEN loop of APN (PDB ID: 4FYQ) and IRAP-closed conformation (PDB ID: 5MJ6) is represented in red, and green respectively, as opposed to the equivalent loop in IRAP (PDB ID: 4PJ6). IRAP is represented in grey color surface and Zn^{2+} is shown as light blue sphere.

conformation adopts a specific, induced fit conformation similar to APN, and in both cases clearly distinct to the IRAP-open structure, and in analogy to our recent findings on IRAP specific cyclic peptide inhibitors.[26]

3. Conclusions

We have prepared and evaluated a new class of IRAP inhibitors synthesized by a simple MW-promoted three-component reaction, or by a two-step-one-pot procedure. Additional structural modifications have been introduced by a rapid Suzuki-Miyaura cross coupling reaction to incorporate various aryl-, heteroaryl- and vinyl-groups in only a few minutes. This spiro-oxindole based class of compounds is one of the few published non-peptidic IRAP inhibitors with sub-μM affinity. They are also selective towards the closely related APN. The computational modeling of these series of compounds suggests that the *S*-configuration of the substituted spiro-oxindole dihydroquinazolinones accounts for the inhibitory capacity within the series. The interactions with the binding cavity in IRAP are thus stereoselective, and the corresponding *R*-configuration is postulated to be essentially inactive in all cases. Furthermore, the proposed binding mode is compatible with the simultaneous binding of L-Leu-*p*NA, in agreement with the uncompetitive IRAP inhibition here determined for a representative compound. As such, this class of compounds represents an interesting starting point for further developments towards *in vivo* candidates. Necessary developments include further improvements in potency, as this is still considerably lower than for the peptide-based inhibitors. The compounds also suffer from poor *in vitro* metabolic stability and most of them have poor solubility, in line with observations for other published small-molecule based IRAP inhibitors.[29] Importantly, compound **40** shows that it is possible to increase the solubility substantially and still maintain a potency comparable to **1**. Efforts to improve the pharmacokinetic properties are ongoing with the aim to transform these IRAP inhibitors into valuable research tools and to enable assessment of their potential as future cognitive enhancers.

Experimental Section

General Information

Microwave heating was performed in a Biotage single-mode microwave reactor producing controlled irradiation at 2450 MHz with a power of 0–400 W. The reaction temperature was determined and controlled using the built-in online IR-sensor. Microwave mediated reactions were performed in septum sealed Biotage vials. Analytical TLC was performed on silica gel 60 F-254 plates and visualized with UV light (λ = 254 nm). Analytical HPLC/ESI-MS was performed on a Dionex UltiMate 3000 HPLC system with a Bruker amazon SL ion trap mass spectrometer and detection by UV (diode array detector, 214, 254 and 280 nm) and electrospray ionization (ESI) MS using a Phenomenex Kinetex C18 column (50 × 3.0 mm, 2.6 μm particle size, 100 Å pore size) with gradients of $H_2O/CH_3CN/0.05\%$ HCOOH as mobile phase at a flow rate of 1.5 mL/min. Purification was performed on column chromatography using silica gel (60–120 mesh size), and for test compounds, as small amount of the final product was purified using reversed-phase high-performance liquid chromatography (RP-HPLC) (UV-triggered (254 nm) fraction collection with a Dionex UltiMate 3000 HPLC system, using an Macherey-Nagel Nucleodur C18 column (21 × 125 mm, 5 μm particle size), and $H_2O/CH_3CN/0.1\%$ CF_3COOH as eluent in a gradient (10 mL/min over 15–20 min)). High resolution molecular masses (HRMS) were determined on a mass spectrometer equipped with an ESI source and 7-T hybrid linear ion trap (LTQ). Nuclear magnetic resonance (NMR) spectra were recorded at 400 MHz for ^1H and 101 MHz for ^{13}C. Chemical shifts (δ) are reported in ppm with the residual solvent peak as internal standard (^1H, $CDCl_3$ 7.26 ppm, CD_3OD 3.31 ppm, DMSO-d_6 2.50 ppm; ^{13}C, $CDCl_3$ 77.16 ppm, CD_3OD 49.00 ppm, DMSO-d_6 39.52 ppm). Coupling constants J are reported in hertz (Hz). All final compounds were ≥95% pure as determined by HPLC (UV at 254 nm) and NMR.

Synthesis, spectral data and analysis of compounds **1**–**3**, **17**, **23**, **26**–**29** and **31** have already been published.[41]

Synthesis of Compounds 4–9, 24–25

General Procedure: *N*-methylated isatin (1 equiv), the appropriate aniline (1.2 equiv) and isatoic anhydride (1.2 equiv) were mixed in acetic acid (0.1 M based on isatin) and heated by microwave irradiation at 150 °C for 10 min (fixed hold time) in a sealed vial. The reaction mixture was cooled to room temperature upon which the product precipitate from the solution. The crude products were filtered and purified by recrystallization from EtOH.

5-Fluoro-1-methyl-3′-(*p*-tolyl)-1′*H*-spiro[indoline-3,2′-quinazoline]-2,4′(3′*H*)-dione (4). 5-Fluoro-1-methylindoline-2,3-dione (200 mg, 1.12 mmol), isatoic anhydride (220 mg, 1.34 mmol), *p*-toluidine (120 mg, 1.34 mmol) and AcOH (11 mL). White powder (300 mg, 66%). ^1H NMR (400 MHz, DMSO-d_6) δ 7.68 (dd, J = 1.5, 7.8 Hz, 1H), 7.63–7.57 (m, 2H), 7.32 (ddd, J = 1.6, 7.3, 8.0 Hz, 1H), 7.12 (ddd, J = 2.7, 8.6, 9.4 Hz, 1H), 7.04–6.99 (m, 2H), 6.92–6.82 (m, 3H), 6.78 (ddd, J = 1.0, 7.4, 8.2 Hz, 1H), 6.69 (dd, J = 1.0, 8.1 Hz, 1H), 3.02 (s, 3H), 2.18 (s, 3H). ^{13}C NMR (101 MHz, DMSO-d_6) δ 173.9, 163.40, 158.4 (d, $J_{C\text{-}F}$ = 241 Hz), 145.8, 139.4 (d, $J_{C\text{-}F}$ = 1.8 Hz), 137.1, 135.1, 133.8, 129.3, 128.4 (d, $J_{C\text{-}F}$ = 7.9 Hz), 127.5, 117.9, 117.3 (d, $J_{C\text{-}F}$ = 24.3 Hz), 114.5, 114.2 (d, $J_{C\text{-}F}$ = 25.2 Hz), 114.1, 110.1 (d, $J_{C\text{-}F}$ = 7.6 Hz), 76.2, 26.1, 20.6. HRMS (ES) *m/z* calcd. for $C_{23}H_{19}FN_3O_2$: $[M+H]^+$ 388.1461, found: 388.1449.

5-Chloro-1-methyl-3′-(*p*-tolyl)-1′*H*-spiro[indoline-3,2′-quinazoline]-2,4′(3′*H*)-dione (5). 5-Chloro-1-methylindoline-2,3-dione (200 mg, 1.02 mmol), isatoic anhydride (110 mg, 1.23 mmol), *p*-toluidine (110 mg, 1.23 mmol) and AcOH (10 mL). White powder (270 mg, 65%). ^1H NMR (400 MHz, DMSO-d_6) δ 7.73 (dd, J = 0.4, 2.2 Hz, 1H), 7.68 (dd, J = 1.6, 7.7 Hz, 1H), 7.63–7.61 (m, 1H), 7.36–7.30 (m, 2H), 7.04–7.00 (m, 2H), 6.91 (dd, J = 0.4, 8.4 Hz, 1H), 6.85 (d, J = 7.9 Hz, 2H), 6.78 (ddd, J = .1, 7.3, 7.8 Hz, 1H), 6.69 (ddd, J = 0.5, 1.1, 8.1 Hz, 1H), 3.02 (s, 3H), 2.19 (s, 3H). ^{13}C NMR (101 MHz, DMSO-d_6) δ 173.8, 163.6, 145.9, 142.2, 137.3, 135.2, 133.9, 130.9, 129.5, 128.7, 127.6, 127.0, 126.4, 118.2, 114.6, 114.3, 110.7, 76.2, 26.2, 20.7. HRMS (ES) *m/z* calcd. for $C_{23}H_{19}ClN_3O_2$: $[M+H]^+$ 404.1166, found: 404.1170.

5-Iodo-1-methyl-3′-(*p*-tolyl)-1′*H*-spiro[indoline-3,2′-quinazoline]-2,4′(3′*H*)-dione (6). 5-Iodo-1-methylindoline-2,3-dione (147 mg, 0.51 mmol), *p*-toluidine (57 mg, 0.61 mmol), isatoic anhydride (98 mg, 0.60 mmol) and AcOH (5 mL). White powder (165 mg, 67%). ^1H NMR (400 MHz, DMSO-d_6) δ 7.92 (d, J = 1.8 Hz, 1H), 7.68 (dd, J = 1.5, 7.8 Hz, 1H), 7.63–7.60 (m, 2H), 7.32 (ddd, J = 1.6, 7.3, 8.1 Hz, 1H), 7.02 (d, J = 8.2 Hz, 2H), 6.83 (d, J = 7.9 Hz, 2H), 6.80–6.76 (m, 1H), 6.73 (d, J = 8.2 Hz, 1H), 6.68 (dd, J = 1.0, 8.1 Hz, 1H), 3.00 (s,

3H), 2.19 (s, 3H). ^{13}C NMR (101 MHz, DMSO-d$_6$) δ 173.3, 163.4, 145.7, 142.9, 139.4, 137.1, 135.1, 134.4, 133.7, 129.3, 129.0, 127.5, 118.0, 114.5, 114.1, 111.5, 85.7, 75.9, 26.0, 20.6. HRMS (ES) *m/z* calcd. for $C_{23}H_{19}IN_3O_2$: $[M+H]^+$ 496.0522, found: 496.0525.

1-Methyl-5-nitro-3′-(*p*-tolyl)-1′*H*-spiro[indoline-3,2′-quinazoline]-2,4′(3′*H*)-dione (7). 1-Methyl-5-nitroindoline-2,3-dione (50 mg, 0.24 mmol), isatoic anhydride (42 mg, 0.26 mmol), *p*-touidine (28 mg, 0.26 mmol) and AcOH (2.4 mL). Off-white powder (56 mg, 56%). ^{1}H NMR (400 MHz, DMSO-d$_6$) δ 8.46 (d, J=2.3 Hz, 1H), 8.24 (dd, J=2.4, 8.7 Hz, 1H), 7.72 (dd, J=1.6, 7.8 Hz, 1H), 7.70 (s, 1H), 7.36 (ddd, J=1.6, 7.3, 8.1 Hz, 1H), 7.14 (d, J=8.7 Hz, 1H), 7.03–6.99 (m, 2H), 6.88–6.85 (m, 2H), 6.83 (ddd, J=1.1, 7.3, 7.8 Hz, 1H), 6.71 (dd, J=1.1, 8.1 Hz, 1H), 3.11 (s, 3H), 2.16 (s, 3H). ^{13}C NMR (101 MHz, DMSO-d$_6$) δ 174.5, 163.2, 149.0, 145.5, 142.9, 137.4, 134.8, 134.0, 129.5, 127.9, 127.8, 127.6, 121.7, 118.4, 114.5, 114.3, 109.7, 75.7, 26.5, 20.6. HRMS (ES) *m/z* calcd. for $C_{23}H_{19}N_4O_2$: $[M+H]^+$ 415.1406, found: 415.1403.

5-Amino-1-methyl-3′-(*p*-tolyl)-1′*H*-spiro[indoline-3,2′-quinazoline]-2,4′(3′*H*)-dione (8). Compound **7** (20 mg, 0.05 mmol) was dissolved in 10 mL EtOH and 7 mL MeOH and Pd/C (10 mol%) were added. The reaction mixture was degassed and flushed with nitrogen three times, and finally filled with H_2-gas. The mixture was stirred for 6 h at ambient temperature, and was subsequently filtered through celite and concentrated in vacou to afford a light yellow powder. ^{1}H NMR (400 MHz, DMSO-d$_6$) δ 7.68 (dt, J=7.9, 1.7 Hz, 1H), 7.59 (s, 1H), 7.36–7.27 (m, 2H), 7.00 (d, J=8.3 Hz, 2H), 6.94 (d, J=8.3 Hz, 1H), 6.85–6.73 (m, 4H), 6.69 (dd, J=8.2, 1.3 Hz, 1H), 2.97 (s, 3H), 2.18 (s, 3H). ^{13}C NMR (101 MHz, DMSO-d$_6$) δ 173.7, 163.9, 146.4, 137.5, 135.5, 134.3, 129.7, 129.3, 128.6, 128.0, 118.4, 114.8, 114.6, 117.9, 110.2, 76.8, 26.5, 21.0. HRMS (ES) *m/z* calcd. for $C_{23}H_{21}N_4O_2$: $[M+H]^+$ 385.1665, found: 385.1676.

5-Methoxy-1-methyl-3′-(*p*-tolyl)-1′*H*-spiro[indoline-3,2′-quinazoline]-2,4′(3′*H*)-dione (9). 5-Methoxy-1-methylindoline-2,3-dione (60 mg, 0.31 mmol), isatoic anhydride (62 mg, 0.38 mmol), *p*-toluidine (41 mg, 0.38 mmol) and AcOH (3 mL). Off-white powder (117 mg, 93%). ^{1}H NMR (400 MHz, DMSO-d$_6$) δ 7.67 (dd, J=1.6, 7.8 Hz, 1H), 7.55 (s, 1H), 7.30 (ddd, J=1.6, 7.3, 8.4 Hz, 1H), 7.26 (d, J=2.4 Hz, 1H), 7.00 (dd, J=1.0, 8.5 Hz, 2H), 6.84 (d, J=8.6 Hz, 2H), 6.81 (d, J=2.5 Hz, 1H), 6.79 (s, 1H), 6.76 (td, J=1.1, 7.6 Hz, 1H), 6.69 (dd, J=1.0, 8.2 Hz, 1H), 3.70 (s, 3H), 2.99 (s, 3H), 2.17 (s, 3H). ^{13}C NMR (101 MHz, DMSO-d$_6$) δ 173.8, 163.7, 155.6, 146.1, 136.9, 136.5, 135.4, 133.7, 129.2, 127.9, 127.5, 117.8, 115.9, 114.6, 114.1, 112.8, 109.7, 76.5, 55.8, 26.0, 20.6. HRMS (ES) *m/z* calcd. for $C_{24}H_{22}N_3O_3$: $[M+H]^+$ 400.1661, found: 400.1658.

3′-(*p*-Tolyl)-1′*H*-spiro[indoline-3,2′-quinazoline]-2,4′(3′*H*)-dione (24). Isatin (147 mg, 1.0 mmol), isatoic anhydride (163 mg, 1.0 mmol), *p*-toluidine (107 mg, 1.0 mmol) and AcOH (10 mL). Off-white powder (252 mg, 71%). ^{1}H NMR (400 MHz, DMSO-d$_6$) δ 10.38 (s, 1H), 7.66 (dd, J=7.8, 1.6 Hz, 1H), 7.58 (s, 1H), 7.54 (dd, J=7.5, 1.2 Hz, 1H), 7.30 (ddd, J=8.5, 7.3, 1.6 Hz, 1H), 7.16 (td, J=7.7, 1.3 Hz, 1H), 7.01 (d, J=8.1 Hz, 2H), 6.94 (td, J=7.5, 1.0 Hz, 1H), 6.86 (d, J=8.1 Hz, 2H), 6.75 (td, J=7.5, 1.0 Hz, 1H), 6.70 (dd, J=8.0, 1.0 Hz, 1H), 6.65 (d, J=7.7 Hz, 1H), 2.18 (s, 3H). ^{13}C NMR (101 MHz, DMSO) δ 175.5, 163.6, 146.1, 141.6, 136.8, 135.4, 133.6, 130.8, 129.2, 127.5, 127.4, 126.4, 122.1, 117.6, 114.6, 114.0, 110.1, 76.4, 20.5. HRMS (ES) *m/z* calcd. for $C_{22}H_{18}N_3O_2$: $[M+H]^+$ 356.1399, found: 356.1412

5-Bromo-1-methyl-1′*H*-spiro[indoline-3,2′-quinazoline]-2,4′(3′*H*)-dione (25). 5-bromo-1-methylindoline-2,3-dione (202 mg, 0.84 mmol), isatoic ahydride (140 mg, 0.86 mmol), NH_4OAc (70 mg, 0.91 mmol) and AcOH (10 mL). Beige powder (301 mg, 45%). ^{1}H NMR (400 MHz, DMSO-d$_6$) δ 8.33 (s, 1H), 7.65–7.61 (m, 3H), 7.29 (s, 1H), 7.25 (ddd, J=1.6, 7.2, 8.1 Hz, 1H), 7.06 (m, 1H), 6.72 (ddd, J=1.0, 7.2, 8.2 Hz, 1H), 6.60 (dd, J=0.9, 8.1 Hz, 1H), 3.07 (s, 3H). ^{13}C NMR (101 MHz, DMSO-d$_6$) δ 173.9, 163.7, 146.5, 142.9, 133.6, 133.6, 131.0, 127.7, 127.0, 117.6, 114.6, 114.2, 114.0, 111.2, 70.8, 26.1. HRMS (ES) *m/z* calcd. for $C_{16}H_{13}N_3O_2Br$: $[M+H]^+$ 358.0191, found: 358.0189.

Synthesis of Compounds 10–16, 18–22

General procedure Suzuki-Miyaura cross-coupling reaction. The appropriate boronic acid/ester (0.45 mmol; for compound **10** 2.24 mmol), compound **1** (0.22 mmol), DBU (0.34 mmol) and $PdCl_2$(dppf) (0.006 mmol, 2.5 mol%) were added to a sealed vial, which was evacuated and backfilled with nitrogen. MeCN (9.8 mL) and H_2O (0.2 mL) were added and the mixture was heated by microwave irradiation for 1 min at 180 °C (fixed hold time). The crude product was concentrated under reduced pressure and purified by silica flash column chromatography.

1,5-Dimethyl-3′-(*p*-tolyl)-1′*H*-spiro[indoline-3,2′-quinazoline]-2,4′(3′*H*)-dione (10). Methylboronic acid. White solid (26 mg, 30%). ^{1}H NMR (400 MHz, DMSO-d$_6$) δ 7.67 (dd, J=1.6, 7.8 Hz, 1H), 7.55 (s, 1H), 7.45 (d, J=1.7 Hz, 1H), 7.30 (ddd, J=1.6, 7.3, 8.2 Hz, 1H), 7.07 (ddd, J=0.9, 1.8, 7.9 Hz, 1H), 6.98 (dd, J=0.8, 8.4 Hz, 2H), 6.80 (d, J=8.4 Hz, 2H), 6.76 (t, J=7.3 Hz, 2H), 6.68 (dd, J=1.0, 8.1 Hz, 1H), 2.98 (s, 3H), 2.23 (s, 3H), 2.17 (s, 3H). ^{13}C NMR (101 MHz, DMSO-d$_6$) δ 173.8, 163.7, 146.1, 140.8, 136.9, 135.4, 133.7, 132.0, 131.1, 129.2, 127.5, 126.9, 126.7, 117.8, 114.5, 114.1, 108.8, 76.3, 26.0, 20.6. HRMS (ES) *m/z* calcd. for $C_{24}H_{22}N_3O_2$: $[M+H]^+$ 384.1712, found: 384.1729.

5-(4-Fluorophenyl)-1-methyl-3′-(*p*-tolyl)-1′*H*-spiro[indoline-3,2′-quinazoline]-2,4′(3′*H*)-dione (11). 4-Fluorophenylboronic acid. Light yellow solid (95.7 mg, 93%). ^{1}H NMR (400 MHz, $CDCl_3$) δ 8.03 (dd, J=1.6, 7.8 Hz, 1H), 7.69 (dd, J=0.5, 1.9 Hz, 1H), 7.45–7.38 (m, 3H), 7.35 (ddd, J=1.6, 7.3, 8.0 Hz, 1H), 7.15–7.08 (m, 2H), 6.99–6.94 (m, 3H), 6.89 (d, J=7.8 Hz, 2H), 6.71 (dd, J=0.5, 8.2 Hz, 1H), 6.65 (ddd, J=0.5, 1.1, 8.0 Hz, 1H), 4.61 (s, 1H), 3.08 (s, 3H), 2.21 (s, 3H). ^{13}C NMR (101 MHz, $CDCl_3$) δ 173.5, 162.6 (d, $J_{C\text{-}F}$=247.6 Hz), 161.4, 156.3, 144.1, 142.3, 138.1, 136.3 (d, $J_{C\text{-}F}$=3.2 Hz), 136.0, 135.0, 134.0, 129.9, 129.8, 129.1, 128.4 (d, $J_{C\text{-}F}$=8.5 Hz), 128.1, 124.3, 120.6, 116.9, 116.0 (d, $J_{C\text{-}F}$=21.5 Hz), 115.0, 109.1, 76.7, 26.4, 21.2. HRMS (ES) *m/z* calcd. for $C_{29}H_{23}FN_3O_2$: $[M+H]^+$ 464.1774, found: 464.1767.

1-Methyl-5-(4-phenoxyphenyl)-3′-(*p*-tolyl)-1′*H*-spiro[indoline-3,2′-quinazoline]-2,4′(3′*H*)-dione (12). 4-Phenoxyphenylboronic acid. Light yellow solid (117 mg, 96%). ^{1}H NMR (400 MHz, DMSO-d$_6$) δ 7.93 (d, J=1.9 Hz, 1H), 7.69 (dd, J=1.6, 7.8 Hz, 1H), 7.67–7.63 (m, 3H), 7.56 (dd, J=1.9, 8.2 Hz, 1H), 7.42 (m, 2H), 7.31 (ddd, J=1.6, 7.3, 8.1 Hz, 1H), 7.17 (tt, J=1.1, 7.4 Hz, 1H), 7.08–7.04 (m, 4H), 6.99 (d, J=8.3 Hz, 2H), 6.94 (d, J=8.2 Hz, 1H), 6.91 (m, 2H), 6.77 (dd, J=1.0, 7.6 Hz, 1H), 6.70 (dd, J=1.0, 8.2 Hz, 1H), 3.06 (s, 3H), 2.15 (s, 3H). ^{13}C NMR (101 MHz, DMSO-d$_6$) δ 174.1, 163.6, 156.5, 156.20, 146.0, 142.4, 136.9, 136.1, 135.4, 134.5, 134.3, 133.6, 130.1, 129.2, 128.9, 127.9, 127.5, 124.2, 119.1, 118.9, 117.8, 117.1, 114.7, 114.1, 109.5, 76.2, 26.1, 20.6. HRMS (ES) *m/z* calcd. for $C_{35}H_{28}N_3O_3$: $[M+H]^+$ 538.2131, found: 538.2143.

***N*-(3-(1-Methyl-2,4′-dioxo-3′-(*p*-tolyl)-3′,4′-dihydro-1′*H*-spiro[indoline-3,2′-quinazolin]-5-yl)phenyl)acetamide (13)**. 3-Acetamidophenylboronic acid. Light yellow solid (89 mg, 80%). ^{1}H NMR (400 MHz, DMSO-d$_6$) δ 10.00 (s, 1H), 7.85 (d, J=2.0 Hz, 2H), 7.70 (dd, J=1.6, 7.7 Hz, 1H), 7.67 (s, 1H), 7.57 (ddd, J=1.1, 2.1, 8.0 Hz, 1H), 7.52 (dd, J=1.9, 8.2 Hz, 1H), 7.36 (m, 1H), 7.34–7.26 (m, 2H), 6.98 (dd, J=8.1, 9.2 Hz, 3H), 6.87 (d, J=8.5 Hz, 2H), 6.78 (td, J=1.1, 7.5 Hz, 1H), 6.71 (dd, J=1.0, 8.1 Hz, 1H), 3.06 (s, 3H), 2.15 (s, 3H), 2.06 (s, 3H). ^{13}C NMR (101 MHz, DMSO-d$_6$) δ 174.1, 168.4, 163.6, 146.0, 142.7, 139.94, 139.82, 137.0, 135.3, 134.9, 133.7, 129.35, 129.26, 129.1, 127.49, 127.46, 124.4, 120.9, 117.8, 117.7, 116.8, 114.5, 114.1, 109.5, 76.2,

26.1, 24.1, 20.5. HRMS (ES) *m/z* calcd. for $C_{31}H_{27}N_4O_3$: $[M+H]^+$ 503.2083, found: 503.2078.

4-(1-Methyl-2,4′-dioxo-3′-(*p*-tolyl)-3′,4′-dihydro-1′*H*-spiro[indoline-3,2′-quinazolin]-5-yl)benzonitrile (14). 4-Cyanophenylboronic acid. Light beige solid (83 mg, 79%). 1H NMR (400 MHz, $CDCl_3$) δ 8.02 (ddd, $J=0.5$, 1.6, 7.8 Hz, 1H), 7.74 (dd, $J=0.5$, 1.9 Hz, 1H), 7.71 (dm, $J=8.7$ Hz, 2H), 7.56 (dm, $J=8.7$ Hz, 2H), 7.50 (dd, $J=1.9$, 8.2 Hz, 1H), 7.35 (ddd, $J=1.6$, 7.3, 8.0 Hz, 1H), 6.99–6.93 (m, 3H), 6.87 (d, $J=7.8$ Hz, 2H), 6.76 (dd, $J=0.5$, 8.2 Hz, 1H), 6.65 (ddd, $J=0.5$, 1.1, 8.0 Hz, 1H), 3.09 (s, 3H), 2.20 (s, 3H). ^{13}C NMR (101 MHz, $CDCl_3$) δ 173.5, 164.2, 144.4, 144.0, 143.6, 138.3, 134.9, 134.7, 134.1, 132.9, 130.4, 129.9, 129.2, 129.0, 128.5, 127.3, 124.5, 120.8, 118.9, 116.8, 115.0, 111.2, 109.4, 76.6, 26.5, 21.2. HRMS (ES) *m/z* calcd. for $C_{30}H_{22}N_4O_2Na$: $[M+H]^+$ 493.1640, found: 493.1645.

5-(2-Ethylphenyl)-1-methyl-3′-(*p*-tolyl)-1′*H*-spiro[indoline-3,2′-quinazoline]-2,4′(3′*H*)-dione (15). 2-Ethylphenylboronic acid. Off-white solid (68 mg, 64%). 1H NMR (400 MHz, CD_3OD including $CDCl_3$) δ 7.85 (dd, $J=7.9$, 1.6 Hz, 1H), 7.42 (d, $J=1.8$ Hz, 1H), 7.37 (s, 1H), 7.29 (ddd, $J=8.8$, 7.3, 1.6 Hz, 1H), 7.27–7.23 (m, 2H), 7.18 (dd, $J=7.7$, 2.6 Hz, 1H), 7.16 (ddd, $J=8.0$, 1.7, 0.6 Hz, 1H), 7.04–7.00 (m, 1H), 6.96 (d, $J=8.0$ Hz, 2H), 6.84 (d, $J=8.0$ Hz, 2H), 6.81 (ddd, $J=8.4$, 7.3, 1.6 Hz, 1H), 6.70 (d, $J=8.1$ Hz, 1H), 6.64 (dd, $J=8.2$, 1.1 Hz, 1H), 3.07 (s, 3H), 2.41 (q, $J=7.5$ Hz, 2H), 2.20 (s, 3H), 0.97 (t, $J=7.5$, 3H). ^{13}C NMR (101 MHz, CD_3OD including $CDCl_3$) δ 174.4, 165.3, 145.4, 141.9, 141.7, 140.5, 138.2, 137.8, 135.0, 134.3, 132.1, 130.0, 129.8, 128.9, 128.6, 128.0, 127.1, 126.8, 125.9, 119.6, 115.7, 114.6, 108.7, 77.1, 26.3, 21.1, 15.6. HRMS (ES) *m/z* calcd. for $C_{31}H_{28}N_3O_2$: $[M+H]^+$ 474.2182, found: 474.2194.

5-(2-Methoxyphenyl)-1-methyl-3′-(*p*-tolyl)-1′*H*-spiro[indoline-3,2′-quinazoline]-2,4′(3′*H*)-dione (16). 2-Methoxyphenylboronic acid. Off-white solid (96 mg, 91%). 1H NMR (400 MHz, DMSO-d_6) δ 7.72 (dd, $J=0.4$, 1.8 Hz, 1H), 7.68 (dd, $J=1.5$, 7.8 Hz, 1H), 7.62 (s, 1H), 7.36 (dd, $J=1.8$, 8.1 Hz, 1H), 7.33 (m, 1H), 7.30 (m, 1H), 7.21 (dd, $J=1.7$, 7.5 Hz, 1H), 7.10 (dd, $J=1.1$, 8.4 Hz, 1H), 7.04–7.00 (m, 3H), 6.91 (dd, $J=0.4$, 8.1 Hz, 1H), 6.87 (d, $J=8.3$ Hz, 2H), 6.77 (ddd, $J=1.0$, 7.4, 8.2 Hz, 1H), 6.69 (dd, $J=0.9$, 8.3 Hz, 1H), 3.77 (s, 3H), 3.04 (s, 3H), 2.18 (s, 3H). ^{13}C NMR (101 MHz, DMSO-d_6) δ 173.9, 163.7, 156.0, 146.1, 142.0, 137.0, 135.3, 133.7, 132.8, 131.7, 130.1, 129.2, 128.9, 128.9, 127.5, 127.0, 126.5, 120.9, 117.9, 114.6, 114.2, 111.9, 108.8, 76.4, 55.6, 26.1, 20.6. HRMS (ES) *m/z* calcd. for $C_{30}H_{26}N_3O_3$: $[M+H]^+$ 476.1974, found: 476.1970.

1-Methyl-5-(pyridin-4-yl)-3′-(*p*-tolyl)-1′*H*-spiro[indoline-3,2′-quinazoline]-2,4′(3′*H*)-dione (18). 4-Pyridinylboronic acid. Yellow solid (70 mg, 70%). 1H NMR (400 MHz, $CDCl_3$) δ 8.64 (dd, $J=4.4$, 1.7 Hz, 2H), 8.05 (dd, $J=7.7$, 1.5 Hz, 1H), 7.80 (dd, $J=2.0$, 0.6 Hz, 1H), 7.56 (dd, $J=8.2$, 1.9 Hz, 1H), 7.39–7.34 (m, 3H), 7.01–6.95 (m, 3H), 6.88 (d, $J=7.8$ Hz, 2H), 6.77 (dd, $J=8.2$, 0.5 Hz, 1H), 6.67 (ddd, $J=8.0$, 1.1, 0.6 Hz, 1H), 4.63 (s, 1H), 3.10 (s, 3H), 2.21 (s, 3H). ^{13}C NMR (101 MHz, $CDCl_3$) δ 173.6, 164.1, 150.6, 147.1, 144.0, 143.9, 138.2, 135.0, 134.1, 133.6, 130.2, 129.9, 129.2, 128.5, 124.3, 121.1, 120.8, 117.0, 115.0, 109.4, 76.5, 26.5, 21.2. HRMS (ES) *m/z* calcd. for $C_{28}H_{23}N_4O_2$: $[M+H]^+$ 447.1821, found: 447.1813.

1-Methyl-5-(quinolin-8-yl)-3′-(*p*-tolyl)-1′H-spiro[indoline-3,2′-quinazoline]-2,4′(3′*H*)-dione (19). 8-Quinolinylboronic acid. Beige solid (87 mg, 79%). 1H NMR (400 MHz, $CDCl_3$) δ 8.92 (dd, $J=4.2$, 1.8 Hz, 1H), 8.22 (dd, $J=8.3$, 1.8 Hz, 1H), 7.99 (dd, $J=7.8$, 1.6 Hz, 1H), 7.94 (d, $J=1.7$ Hz, 1H), 7.83 (dt, $J=7.3$, 3.7 Hz, 1H), 7.63–7.57 (m, 3H), 7.44 (dd, $J=8.3$, 4.2 Hz, 1H), 7.31 (ddd, $J=8.0$, 7.3, 1.6 Hz, 1H), 7.06–6.99 (m, 4H), 6.89 (td, $J=7.6$, 1.1 Hz, 1H), 6.75 (d, $J=8.1$ Hz, 1H), 6.62 (dd, $J=8.0$, 1.0 Hz, 1H), 3.09 (s, 3H), 2.22 (s, 3H). HRMS (ES) *m/z* calcd. for $C_{32}H_{25}N_4O_2$: $[M+H]^+$ 497.1978, found: 497.1980.

1-Methyl-5-(thiophen-2-yl)-3′-(*p*-tolyl)-1′*H*-spiro[indoline-3,2′-quinazoline]-2,4′(3′*H*)-dione (20). 2-Thienylboronic acid. Light beige solid (43 mg, 43%). 1H NMR (400 MHz, DMSO-d_6) δ 7.94 (dd, $J=0.5$, 2.0 Hz, 1H), 7.70 (dd, $J=1.6$, 7.7 Hz, 1H), 7.65 (s, 1H), 7.53 (dd, $J=2.0$, 8.2 Hz, 1H), 7.51 (dd, $J=1.2$, 3.6 Hz, 1H), 7.49 (dd, $J=1.1$, 5.1 Hz, 1H), 7.32 (ddd, $J=1.6$, 7.2, 8.1 Hz, 1H), 7.11 (dd, $J=3.6$, 5.1 Hz, 1H), 6.99 (d, $J=8.5$ Hz, 2H), 6.91 (dd, $J=0.5$, 8.2 Hz, 1H), 6.88 (d, $J=8.1$ Hz, 2H), 6.78 (ddd, $J=1.1$, 7.3, 8.3 Hz, 1H), 6.70 (ddd, $J=0.5$, 1.1, 8.2 Hz, 1H), 3.05 (s, 3H), 2.15 (s, 3H). ^{13}C NMR (101 MHz, DMSO-d_6) δ 174.0, 163.6, 145.9, 142.8, 142.5, 137.0, 135.3, 133.7, 129.3, 128.9, 128.6, 128.0, 127.6, 127.5, 125.1, 123.3, 117.9, 114.6, 114.1, 109.6, 76.1, 26.1, 20.5. HRMS (ES) *m/z* calcd. for $C_{27}H_{22}N_3O_2S$: $[M+H]^+$ 452.1433, found: 452.1439.

1-Methyl-3′-(*p*-tolyl)-5-vinyl-1′*H*-spiro[indoline-3,2′-quinazoline]-2,4′(3′*H*)-dione (21). 2,4,6-Trivinylcyclotriboroxane pyridine complex. Beige solid (84 mg, 95%). 1H NMR (400 MHz, DMSO-d_6) δ 7.82 (d, $J=1.8$ Hz, 1H), 7.68 (dd, $J=1.6$, 7.7 Hz, 1H), 7.59 (s, 1H), 7.35–7.28 (m, 2H), 6.98 (dd, $J=0.9$, 8.2 Hz, 2H), 6.86–6.81 (m, 3H), 6.77 (ddd, $J=1.1$, 7.3, 7.8 Hz, 1H), 6.71–6.62 (m, 2H), 5.79 (dd, $J=0.9$, 17.7 Hz, 1H), 5.16 (dd, $J=0.9$, 10.9 Hz, 1H), 3.02 (s, 3H), 2.16 (s, 3H). ^{13}C NMR (101 MHz, DMSO-d_6) δ 174.1, 163.7, 146.0, 142.8, 137.0, 136.0, 135.3, 133.7, 132.4, 129.3, 127.5, 127.2, 123.7, 117.9, 114.6, 114.1, 113.1, 109.0, 76.2, 26.1, 20.6. HRMS (ES) *m/z* calcd. for $C_{25}H_{22}N_3O_2$: $[M+H]^+$ 396.1712, found: 396.1723.

(*E*)-1-Methyl-5-styryl-3′-(*p*-tolyl)-1′*H*-spiro[indoline-3,2′-quinazoline]-2,4′(3′*H*)-dione (22). *E*-Styrylboronic acid. Light pink solid (61 mg, 58%). 1H NMR (400 MHz, CD_3OD and $CDCl_3$) δ 7.86 (ddd, $J=0.5$, 1.6, 7.8 Hz, 1H), 7.74 (d, $J=1.7$ Hz, 1H), 7.46 (m, 2H), 7.38 (dd, $J=1.8$, 8.2 Hz, 1H), 7.35–7.29 (m, 3H), 7.23 (m, 1H), 7.00 (d, $J=3.3$ Hz, 2H), 6.96 (m, 2H), 6.87–6.81 (m, 3H), 6.68 (ddd, $J=0.5$, 1.1, 8.1 Hz, 1H), 6.67 (d, $J=8.2$ Hz, 1H), 3.03 (s, 3H), 2.18 (s, 3H). ^{13}C NMR (101 MHz, CD_3OD and $CDCl_3$) δ 174.6, 165.8, 146.1, 142.6, 138.6, 137.5, 135.0, 134.7, 133.8, 130.1, 130.0, 129.1, 128.7, 128.4, 128.4, 128.1, 127.9, 126.8, 123.7, 119.5, 115.4, 114.8, 109.5, 77.5, 26.4, 21.1. HRMS (ES) *m/z* calcd. for $C_{31}H_{26}N_3O_2$: $[M+H]^+$ 472.2025, found: 472.2037.

Synthesis of Compounds 30, 32–41

General Procedure – Step 1: A mixture of isatoic anhydride (1.2 mmol) and the appropriate amine (1.2 mmol) in a solution of 5% AcOH in EtOH (10 mL) was heated by MW irradiation at 150 °C for 10 min (fixed hold time) in a sealed vial. The solvent was removed under reduced pressure and the intermediate used in the next step without further purification.

General Procedure – Step 2: 5-Br-*N*-Me-isatin (0.48 mmol) was dissolved in 1% TFA in EtOH (5 mL) and the product from step 1 (0.48 mmol) was added. The mixture was heated by MW irradiation at 150 °C for 40 min (fixed hold time). The mixture was allowed to cool to ambient temperature whereupon the product precipitates from the solution. The precipitate was filtered off and purified by silica flash column chromatography.

3′-(4-(Benzyloxy)phenyl)-5-bromo-1-methyl-1′*H*-spiro[indoline-3,2′-quinazoline]-2,4′(3′*H*)-dione (30). 4-Benzyloxyaniline. White powder (180 mg, 79%). 1H NMR (400 MHz, DMSO-d_6) δ 7.82 (d, $J=2.0$ Hz, 1H), 7.68 (dd, $J=1.6$, 7.8 Hz, 1H), 7.61 (s, 1H), 7.48 (dd, $J=2.1$, 8.3 Hz, 1H), 7.41–7.30 (m, 6H), 6.91–6.82 (m, 5H), 6.78 (ddd, $J=1.1$, 7.3, 8.3 Hz, 1H), 6.68 (dd, $J=1.0$, 8.3 Hz, 1H), 4.99 (s, 2H), 3.00 (s, 3H). ^{13}C NMR (101 MHz, DMSO-d_6) δ 173.6, 163.5, 157.5, 145.8, 142.5, 136.7, 133.8, 133.7, 130.4, 129.1, 128.9, 128.4, 127.93, 127.86, 127.6, 118.0, 114.8, 114.6, 114.5, 114.2, 111.2, 76.2, 69.3, 26.1. HRMS (ES) *m/z* calcd. for $C_{29}H_{23}BrN_3O_3$: $[M+H]^+$ 540.0923, found: 540.0926.

3′-Benzyl-5-bromo-1-methyl-1′*H*-spiro[indoline-3,2′-quinazoline]-2,4′(3′*H*)-dione (32). Benzylamine. White powder (130 mg, 53%). 1H

NMR (400 MHz, DMSO-d_6) δ 7.76 (dd, J=6.7, 1.1, 1H), 7.63 (dd, J=8.4, 2.1, 1H), 7.44 (s, 1H), 7.39 (d, J=2.0, 1H), 7.27 (ddd, J=8.3, 7.1, 1.5, 1H), 7.17–7.12 (m, 3H), 6.97 (d, J=8.4, 1H), 6.82–6.76 (m, 3H), 6.62 (d, J=8.1, 1H), 4.43–4.31 (m, 2H), 2.78 (s, 3H). ^{13}C NMR (101 MHz, DMSO-d_6) δ 173.1, 163.9, 145.8, 143.3, 137.0, 134.3, 133.7, 129.1, 128.0, 127.9, 127.8, 127.7, 127.3, 118.3, 114.8, 114.6, 114.3, 111.6, 74.6, 45.7, 26.03. HRMS (ES) *m/z* calcd. for $C_{23}H_{19}BrN_3O_2$: $[M+H]^+$ 448.0661, found: 448.0669.

5-Bromo-1-methyl-3′-phenethyl-1′*H*-spiro[indoline-3,2′-quinazoline]-2,4′(3′*H*)-dione (33). Phenylethylamine. Beige solid (380 mg, 82%). ^{1}H NMR (400 MHz, DMSO-d_6) δ 7.74 (dd, J=2.1, 8.4 Hz, 1H), 7.71 (dd, J=1.6, 7.7 Hz, 1H), 7.68 (dd, J=0.4, 2.0 Hz, 1H), 7.47 (s, 1H), 7.28 (ddd, J=1.6, 7.3, 8.1 Hz, 1H), 7.25–7.19 (m, 2H), 7.18–7.13 (m, 2H), 6.88–6.84 (m, 2H), 6.77 (ddd, J=1.0, 7.2, 7.7 Hz, 1H), 6.62 (ddd, J=0.5, 1.1, 8.1 Hz, 1H), 3.39–3.33 (m, 1H), 3.11 (s, 3H), 2.79 (ddd, J=5.5, 10.5, 12.7 Hz, 1H), 2.70 (td, J=5.0, 10.8, 11.5 Hz, 1H), 2.66–2.58 (m, 1H). ^{13}C NMR (101 MHz, DMSO-d_6) δ 173.1, 163.3, 145.4, 143.1, 138.5, 134.2, 133.5, 128.7, 128.5, 128.23, 128.21, 127.2, 126.3, 118.0, 114.8, 114.3, 113.9, 111.7, 75.2, 45.0, 34.3, 26.2. HRMS (ES) *m/z* calcd. for $C_{24}H_{21}N_3O_2Br$: $[M+H]^+$ 462.0817, found: 462.0826.

5-Bromo-3′-(cyclohexylmethyl)-1-methyl-1′*H*-spiro[indoline-3,2′-quinazoline]-2,4′(3′*H*)-dione (34). Cyclohexylmethylamine. Beige solid (291 mg, 64%). ^{1}H NMR (400 MHz, DMSO-d_6) δ 7.74–7.70 (m, 2H), 7.66 (dd, J=1.6, 7.8 Hz, 1H), 7.42 (s, 1H), 7.26 (ddd, J=1.6, 7.3, 8.1 Hz, 1H), 7.14 (dd, J=2.0, 7.1 Hz, 1H), 6.75 (td, J=1.1, 7.5 Hz, 1H), 6.60 (dd, J=1.0, 8.1 Hz, 1H), 3.11 (s, 3H), 3.06 (dd, J=6.7, 13.8 Hz, 1H), 2.71 (dd, J=7.7, 13.8 Hz, 1H), 1.61–1.48 (m, 3H), 1.43–1.34 (m, 2H), 1.15–1.05 (m, 1H), 1.04–0.85 (m, 3H), 0.80–0.61 (m, 2H). ^{13}C NMR (101 MHz, DMSO-d_6) δ 173.1, 163.8, 145.3, 143.0, 134.1, 133.3, 128.6, 128.6, 127.4, 117.9, 114.7, 114.5, 113.9, 111.6, 74.9, 48.4, 37.3, 30.6, 30.5, 26.2, 25.8, 25.6. HRMS (ES) *m/z* calcd. for $C_{23}H_{25}N_3O_2Br$: $[M+H]^+$ 454.1130, found: 454.1126.

5-Bromo-1-methyl-3′-(pyridin-2-ylmethyl)-1′*H*-spiro[indoline-3,2′-quinazoline]-2,4′(3′*H*)-dione (35). 2-Picolylamine. Beige solid (270 mg, 60%). ^{1}H NMR (400 MHz, DMSO-d_6) δ 8.41 (dt, J=1.3, 5.1 Hz, 1H), 7.90 (td, J=1.8, 7.7 Hz, 1H), 7.71 (dd, J=1.6, 7.8 Hz, 1H), 7.57 (dd, J=2.1, 8.4 Hz, 1H), 7.54 (s, 1H), 7.41–7.36 (m, 2H), 7.35 (d, J=2.0 Hz, 1H), 7.32 (ddd, J=1.6, 7.3, 8.7 Hz, 1H), 7.04 (d, J=8.4 Hz, 1H), 6.79 (td, J=1.1, 7.5 Hz, 1H), 6.65 (dd, J=0.9, 8.1 Hz, 1H), 4.80 (d, J=16.2 Hz, 1H), 4.04 (d, J=16.2 Hz, 1H), 3.02 (s, 3H). ^{13}C NMR (101 MHz, DMSO-d_6) δ 172.7, 163.7, 155.8, 146.4, 145.7, 143.1, 139.2, 134.2, 133.9, 128.5, 127.9, 127.6, 123.2, 122.8, 118.2, 114.5, 114.1, 113.9, 111.7, 75.2, 46.6, 26.2. HRMS (ES) *m/z* calcd. for $C_{22}H_{18}N_4O_2Br$: $[M+H]^+$ 449.0613, found: 449.0619.

5-Bromo-1-methyl-3′-(pyridin-3-ylmethyl)-1′*H*-spiro[indoline-3,2′-quinazoline]-2,4′(3′*H*)-dione (36). 3-Picolylamine. Beige solid (271 mg, 60%). ^{1}H NMR (400 MHz, DMSO-d_6) δ 8.63 (dd, J=1.5, 5.4 Hz, 1H), 8.26 (d, J=2.1 Hz, 1H), 7.84 (dt, J=1.8, 8.2 Hz, 1H), 7.74 (dd, J=1.6, 7.8 Hz, 1H), 7.68–7.62 (m, 2H), 7.57 (s, 1H), 7.43 (d, J=2.0 Hz, 1H), 7.32 (ddd, J=1.6, 7.3, 8.1 Hz, 1H), 7.09 (d, J=8.4 Hz, 1H), 6.80 (td, J=1.1, 7.4 Hz, 1H), 6.64 (dd, J=1.0, 8.2 Hz, 1H), 4.61 (d, J=16.0 Hz, 1H), 4.24 (d, J=16.0 Hz, 1H), 2.96 (s, 3H). ^{13}C NMR (101 MHz, DMSO-d_6) δ 172.6, 163.9, 158.4, 158.1, 145.6, 144.2, 142.9, 140.5, 135.7, 134.3, 134.0, 128.6, 127.7, 127.6, 125.1, 118.1, 114.6, 114.1, 113.6, 111.9, 75.0, 43.1, 26.1. HRMS (ES) *m/z* calcd. for $C_{22}H_{18}N_4O_2Br$: $[M+H]^+$ 449.0613, found: 449.0617.

5-Bromo-3′-(furan-2-ylmethyl)-1-methyl-1′*H*-spiro[indoline-3,2′-quinazoline]-2,4′(3′*H*)-dione (37). Furfurylamine. Beige solid (277 mg, 63%). ^{1}H NMR (400 MHz, DMSO-d_6) δ 7.71 (dd, J=7.8, 1.6 Hz, 1H), 7.67 (dd, J=8.4, 2.1 Hz, 1H), 7.58 (d, J=2.0 Hz, 1H), 7.45 (s, 1H), 7.40 (dd, J=1.8, 0.8 Hz, 1H), 7.27 (ddd, J=8.1, 7.3, 1.6 Hz, 1H), 7.05 (d, J=8.4 Hz, 1H), 6.77 (ddd, J=7.7, 7.2, 1.1 Hz, 1H), 6.61 (ddd, J=8.1, 1.1, 0.5 Hz, 1H), 6.23 (dd, J=3.2, 1.8 Hz, 1H), 5.80 (dd, J=3.2, 0.9 Hz, 1H), 4.58 (dd, J=15.8, 0.8 Hz, 1H), 4.21 (d, J=15.9 Hz, 1H), 2.93 (s, 3H). ^{13}C NMR (101 MHz, DMSO-d_6) δ 172.4, 163.1, 149.7, 145.5, 143.3, 142.3, 134.1, 133.6, 128.4, 127.7, 127.5, 118.1, 114.6, 114.5, 114.1, 111.4, 110.3, 108.6, 74.3, 38.3, 26.0. HRMS (ES) *m/z* calcd. for $C_{21}H_{16}N_3O_3BrNa$: $[M+H]^+$ 460.0273, found: 460.0287.

5-Bromo-3′-butyl-1-methyl-1′*H*-spiro[indoline-3,2′-quinazoline]-2,4′(3′*H*)-dione (38). Butylamine. Beige solid (290 mg, 70%). ^{1}H NMR (400 MHz, DMSO-d_6) δ 7.74–7.69 (m, 2H), 7.66 (dd, J=1.6, 7.7 Hz, 1H), 7.42 (s, 1H), 7.26 (ddd, J=1.6, 7.2, 8.1 Hz, 1H), 7.15 (dd, J=0.6, 8.2 Hz, 1H), 6.74 (td, J=1.1, 7.4 Hz, 1H), 6.59 (dd, J=1.0, 8.1 Hz, 1H), 3.12 (s, 3H), 3.07 (m, 1H), 2.78 (m, 1H), 1.31 (m, 1H), 1.19 (m, 1H), 1.04 (m, 2H), 0.65 (t, J=7.3 Hz, 3H). ^{13}C NMR (101 MHz, DMSO-d_6) δ 173.2, 163.1, 145.3, 142.9, 134.1, 133.3, 128.9, 128.2, 127.2, 117.9, 114.7, 114.4, 113.8, 111.7, 75.0, 42.5, 30.1, 26.2, 19.4, 13.3. HRMS (ES) *m/z* calcd. for $C_{20}H_{21}N_3O_2Br$: $[M+H]^+$ 414.0817, found: 414.0816.

5-Bromo-3′-(2-methoxyethyl)-1-methyl-1′*H*-spiro[indoline-3,2′-quinazoline]-2,4′(3′*H*)-dione (39). 2-Methoxyethylamine. Beige solid (260 mg, 63%). ^{1}H NMR (400 MHz, DMSO-d_6) δ 7.73 (d, J=2.1 Hz, 1H), 7.69 (dd, J=8.4, 2.1 Hz, 1H), 7.66 (dd, J=7.8, 1.5 Hz, 1H), 7.41 (s, 1H), 7.26 (ddd, J=8.3, 7.4, 1.6 Hz, 1H), 7.10 (d, J=8.4 Hz, 1H), 6.75 (td, J=7.5, 1.0 Hz, 1H), 6.60 (dd, J=8.4, 2.1 Hz, 1H), 3.30–3.21 (m, 3H), 3.20–3.11 (m, 1H), 3.09 (s, 3H), 2.97 (s, 3H). ^{13}C NMR (101 MHz, DMSO-d_6) δ 172.9, 163.6, 145.3, 143.4, 134.0, 133.4, 128.5, 128.4, 127.2, 117.9, 114.6, 114.5, 113.9, 111.5, 75.1, 69.9, 57.8, 42.6, 26.2. HRMS (ES) *m/z* calcd. for $C_{19}H_{19}N_3O_3Br$: $[M+H]^+$ 416.0610, found: 416.0609

5-Bromo-3′-(2-(dimethylamino)ethyl)-1-methyl-1′*H*-spiro[indoline-3,2′-quinazoline]-2,4′(3′*H*)-dione (40). Dimethylethylenediamine. Beige solid (240 mg, 56%). ^{1}H NMR (400 MHz, DMSO-d_6) δ 7.79 (d, J=2.0 Hz, 1H), 7.74 (dd, J=8.4, 2.0 Hz, 1H), 7.70 (dd, J=7.8, 1.5 Hz, 1H), 7.59 (s, 1H), 7.32 (ddd, J=8.4, 7.4, 1.5 Hz, 1H), 7.19 (d, J=8.4 Hz, 1H), 6.79 (td, J=7.5, 0.7 Hz, 1H), 6.63 (dd, J=8.2, 0.7 Hz, 1H), 3.55–3.43 (m, 1H), 3.14 (s, 3H), 3.08–2.98 (m, 3H), 2.73 (s, 6H). ^{13}C NMR (101 MHz, DMSO-d_6) δ 172.4, 164.2, 145.4, 142.9, 134.5, 134.2, 128.5, 127.7, 127.3, 118.1, 115.1, 114.1, 113.3, 112.2, 75.6, 55.0, 43.1, 42.3, 38.2, 26.4. HRMS (ES) *m/z* calcd. for $C_{20}H_{22}N_4O_2Br$: $[M+H]^+$ 429.0926, found: 429.0909

5-Bromo-3′-(3-(dimethylamino)propyl)-1-methyl-1′*H*-spiro[indoline-3,2′-quinazoline]-2,4′(3′*H*)-dione (41). 3-Dimethylaminopropylamine. Beige solid (230 mg, 52%). ^{1}H NMR (400 MHz, DMSO-d_6) δ 7.83 (d, J=2.1 Hz, 1H), 7.73 (dd, J=8.4, 2.1 Hz, 1H), 7.68 (dd, J=7.8, 1.5 Hz, 1H), 7.51 (s, 1H), 7.29 (ddd, J=8.7, 7.3, 1.6 Hz, 1H), 7.18 (d, J=8.4 Hz, 1H), 6.76 (td, J=7.5, 1.0 Hz, 1H), 6.62 (dd, J=8.1, 1.0 Hz, 1H), 3.27 (dt, J=14.3, 7.1 Hz, 1H), 2.95 (p, J=5.7 Hz, 2H), 2.81 (dt, J=13.9, 6.8 Hz, 1H), 2.69 (dd, J=11.5, 4.6 Hz, 6H), 1.64 (p, J=7.3 Hz, 2H). ^{13}C NMR (101 MHz, DMSO-d_6) δ 173.0, 164.0, 145.4, 142.9, 134.3, 133.8, 128.7, 128.1, 127.3, 118.0, 115.0, 113.9, 113.8, 112.0, 75.3, 54.4, 42.1, 41.9, 26.3, 23.5. HRMS (ES) *m/z* calcd. for $C_{21}H_{24}N_4O_2Br$: $[M+H]^+$ 443.1083, found: 443.1093

Chiral Separation of Compound 32

Analytical run. Supercritical fluid chromatography (SFC) analysis was performed on a SFC system connected to a back pressure regulator and a PDA detector. The sample was diluted to a concentration of around 1 mg/mL and 10 µL was injected to a 5 µm CHIRALPAK-ID, 4.6×150 mm (diameter×length) column held at 45 °C. An isocratic condition of 35% MeOH in CO_2 was applied at a flow rate of 5 mL/min. The back pressure was set to 120 bar. The PDA scanned from 220 to 400.

Preparative run. The enantiomers of **32** were separated by preparative SFC. The sample for chiral separation was prepared by dissolving 20 mg in 600 μL MeOH and the preparative run was performed by stacked injections on a SFC system connected to a PDA detector. The column used was a 5 μm CHIRALPAK-ID, 10× 250 mm (diameter×length) column held at 45 °C. An isocratic condition of 35% MeOH in CO_2 was applied at a flow rate of 15 mL/min. The back pressure was set to 120 bar. The PDA scanned from 220 to 400 and the enantiomers were collected in separated fractions (with the aid of 2 mL/min of MeOH as make up solvent for the collection) and pooled from each injection.

Molecular Modelling

The crystal structure of human IRAP was retrieved from the protein data bank (PDB code 4PJ6)[45] and prepared as previously described for docking and molecular dynamics (MD) simulations, including protonation and fixing sidechain rotamers.[26] The ligands **1**, **3**, **12**, **24**, **32**, **38** and **40** were built in their most probable 3D conformation using Maestro Molecular Modelling Interface version 10.3 (Schrödinger, LLC; NY). The LigPrep module was used to generate separate versions for their *S* and *R* configuration.

Docking and Molecular Dynamics Simulations

A thorough docking exploration was conducted using Glide[46] in the extra-precision (XP) mode, performing independent explorations for each isomeric form of the molecule on three areas of the IRAP inner crevice, with cubic grids of 30 Å size on each axis, centred at different points: One grid covered the so-called H-site, with centre on the equivalent position of the binding site of the Cα atom of His4 in Ang IV as previously determined.[26] The next area was the Z-site (close to Zn^{2+} site centred at x = 28.98, y = 2.14, z = 76.40) and finally, we also explored a putative A-site (allosteric site, away from Zn^{2+}) with centre at x = 30.97, y = −1.41, z = 59.52. Docking on the Z and A sites was performed using ligand-based core constraints (Core SMARTS: "c1cccc(NC2)c1 C23NCc4c(N3)cccc4") while no core constraints were used in H-site docking calculations. Ligands were ranked using XP-Glide scoring function,[47] which can be written as

$$\text{GlideScoreXP} = \text{Ecoul} + \text{EvdW} + \text{Ebind} + \text{Epenalty} \quad (1)$$

Where the favourable and non-favourable terms for binding are grouped into E_{bind} and $E_{penalty}$ respectively.

MD simulations of the IRAP-**38** complex as determined in binding site Z were performed using the Q[48] program and the OPLS-AA force field there implemented.[49] Parameters for the Zn^{2+} ion and ligand **38** were retrieved from the automatic parametrization available in Macromodel, version 10.3 (Schrödinger LLC). Simulations were done under spherical boundary conditions, with a simulation sphere of 25 Å radius centred on the equivalent position of the Cα atom of His^4 in Ang IV.[26,32,33] This sphere was solvated with TIP3P water molecules[50] and subjected to polarization and radial constraints according to the surface constrained all-atom solvent model[48,51] to mimic the properties of bulk water at the sphere surface. Protein atoms outside the simulation sphere were restrained to their initial positions and only interacted with the system through their bonded terms. All ionizable residues within 20 Å of the Zn^{2+} ion were treated in their charged form, and from those within the outer sphere layer the following residues were also considered with their formal charge, respecting established ionic pairs: Lys520, Lys726, Glu767, Asp773, Arg817, Glu818, Arg820, Glu825, Arg858, Glu887, Lys890, Lys892, Glu895, Arg933, and Glu1002, which result in an overall neutral simulation sphere.[26,32,33] During a 175 ps equilibration stage, the system was slowly heated to the target temperature of 310 K while initial positional restrains on all solute heavy atoms were gradually released. The subsequent MD production phase consisted of 5 replica simulations of 2 ns each, with randomized initial velocities, accounting for a total of 10 ns sampling trajectories. A time step of 1 fs was used, and no positional restraints were applied. Solvent bonds and angles were constrained using the SHAKE algorithm.[43]

Biological Methods

Overexpression of Human IRAP and Aminopeptidase N

Overexpression of human IRAP and aminopeptidase N (APN) was achieved in Freestyle HEK293-F Cells (Invitrogen R790-07). The cells were grown in 80 ml of Freestyle Expression Medium (Invitrogen 12338–018) in 250 ml Erlenmeyer flasks (Corning 431144.40). The flasks were kept at 37 °C, 8% CO_2, 70% relative humidity and with shaking at 130–135 rpm in an Infors Multitron incubator. The cells were transfected with 1.1 μg IRAP overexpressing plasmid/10^6 cells[30] or 0.7 μg APN overexpressing plasmid[17] (kindly provided Dr. Alexandros Nikolau at Vrije Universiteit Brussels, Brussels, Belgium)/10^6 cells in the presence of 2 μg polyethyleneimine/10^6 cells (Polyethyleneimine, linear, MW-25 000, Cat. No. 23966, Polysciences). Prior to overexpression, the plasmids were transfected and propagated in Mach1 E.coli (Invitrogen C8620-03). The plasmid DNA was prepared using QIAGEN Plasmid Plus Maxi Kit (12963). 48 h post-transfection, the cells were harvested by centrifugation at 130×g for 3 min. The cells were washed once with PBS and the cell pellets were stored at −20 °C until used for membrane preparations.

Membrane Preparations

All experiments were based on membrane preparations from either CHO cells or HEK293T suspension cells overexpressing human IRAP or APN. Membrane preparation was achieved essentially as described previously[52] using the following procedure. Washed cell pellets were taken out of the −20 °C freezers and quickly thawed and then placed on ice. Pellets were resuspended in ice-cold 50 mM Tris-HCl at pH 7.4 supplemented with 0.1 mM of phenylmethanesulfonyl fluoride (PMSF; Sigma-Aldrich 78830) and then sonicated for 3×15 sec with 30 sec interruption time using a Branson Digital sonifier 250. The sonicated cells were then transferred to a Dounce homogenizer and homogenized by a minimum of 20 strokes while keeping everything on ice. The homogenate was thereafter transferred to ice-cold tubes and centrifuged at 4 °C and 30.000×g for 30 min. The supernatant was discarded and the membranes were resuspended in buffer and again homogenized using the Dounce homogenizer (20 strokes) and thereafter centrifuged as described above. This procedure was repeated twice and the final membrane pellets from CHO cells were then kept frozen at −20 °C until used. A slightly modified procedure was applied for the HEK293T cell pellets, where the membrane suspension from the second was aliquoted into separate vials and kept frozen at −80 °C until the day of use. Prior to addition to the microplates the thawed membrane suspensions were homogenized in a Dounce homogenizer.

Concentration-Response Experiments in 96-Well Format.

Details for the assay used to evaluate the inhibitory activity of the compounds have already been published.[30] In short:

Concentration-response experiments were performed in transparent 96-well microtiter plates (Nunc, product no. 269620) using membrane preparations from CHO-cells, known to abundantly express IRAP and contain minimal contaminating APN activities. The extent of enzymatic activity in each sample was quantified using the peptide L-Leu-p-nitroanilid (L-Leu-pNA, Sigma-Aldrich, product no. L9125), which upon IRAP-mediated cleavage of the N-terminal amide bond produces p-nitroaniline that absorbs at 405 nm. The final assay volume was 200 μL in an assay buffer consisting of 50 mM Tris-HCl, 150 mM NaCl and 0.1 mM phenylmethanesulfonylfluoride (PMSF) at pH 7.4. The assay was conducted in the presence of a final concentration of 1 mM L-Leu-pNA. Concentration-response experiments using the human orthologue of IRAP or human APN were conducted using the identical set-up as for the absorbance based CHO cell membranes assay. Aliquots of membranes from HEK293 suspension cells overexpressing IRAP or APN were thawed, suspended in assay buffer, homogenized using the Dounce homogenizer and diluted with assay buffer.

Competitions Studies of Compound 32

The enzyme kinetics experiments were performed essentially as described for the inhibitory experiments, except that the substrate concentrations were 0.1, 0.2, 0.3, 0.4, 0.8, 1.6 and 2.8 mM. The serial dilution of the compound stock solution was reproduced across all eight rows of the 96-well plates, and four technical replicates were obtained at each substrate concentration by adding the same substrate solution to four rows on a total of four different plates. These plates were then measured every ten minutes to follow the enzymatic reaction over time. Data obtained in the presence of 150 μM inhibitor was used to define maximal IRAP inhibition, *i.e.* this slope was subtracted from those obtained at lower inhibitor concentrations. Data was fitted to a model for uncompetitive inhibition within GraphPad and compared with models for competitive and non-competitive binding. The uncompetitive inhibition model explains the experimental data with a probability of 99.8%, compared to 0.2% and <0.01% for non-competitive and competitive inhibition, respectively. For illustration purposes data at all inhibitor concentrations were also separately fitted to the Michaelis Menten equation, resulting in the expected parallel decreases in K_m and V_{max} values with increasing inhibitor concentration.

Compound Profiling

Preclinical profiling of the compounds was performed at AstraZeneca in Gothenburg, applying an integrated panel of assays referred to as the DMPK Wave 1 panel. The panel consists of two metabolic stability assays based on rat hepatocytes and human liver microsomes, respectively, a logD assay investigating partitioning between an aqueous solution and octanol, a solubility assay in PBS at pH 7.4 and a plasma protein binding assay performed in human serum and reporting both the fraction unbound and stability of the compounds. All assays are run in an automated 96-well format with a UPLC-MS/MS read-out.[53]

Acknowledgements

The work described herein was supported by Uppsala University, the Swedish Research Council, the Kjell and Märta Beijer Foundation, the Swedish Brain Foundation, and King Gustaf V:s and Queen Victoria's Foundation of Freemasons. Computing time from the Swedish National infrastructure for Computation (SNIC) is acknowledged. We thank Dr. Jonas Brånalt and the Wave 1 team at AstraZeneca R&D in Gothenburg for help with compound registration and testing of preclinical properties. We thank Leif Dahllund at SciLifeLab Drug Discovery and Development platform for help with expression of human IRAP and APN. We thank Camilo Persson for skillful assistance in the chemistry lab.

Keywords: enzymes · inhibitors · insulin-regulated aminopeptidases · preclinical profiling · spiro compounds

[1] J. Braszko, G. Kupryszewski, B. Witczuk, K. Wiśniewski, *Neuroscience* **1988**, *27*, 777–783.
[2] J. W. Harding, V. I. Cook, A. V. Miller-Wing, J. M. Hanesworth, M. F. Sardinia, K. L. Hall, J. W. Stobb, G. N. Swanson, J. K. M. Coleman, J. W. Wright, E. C. Harding, *Brain Res.* **1992**, *583*, 340–343.
[3] K. A. Roberts, L. T. Krebs, E. A. Kramár, M. J. Shaffer, J. W. Harding, J. W. Wright, *Brain Res.* **1995**, *682*, 13–21.
[4] I. Moeller, S. Y. Chai, B. J. Oldfield, M. J. McKinley, D. Casley, F. A. O. Mendelsohn, *Brain Res.* **1995**, *701*, 301–306.
[5] H. Matsumoto, T. Rogi, K. Yamashiro, S. Kodama, N. Tsuruoka, A. Hattori, K. Takio, S. Mizutani, M. Tsujimoto, *Eur. J. Biochem.* **2000**, *267*, 46–52.
[6] H. Matsumoto, T. Nagasaka, A. Hattori, T. Rogi, N. Tsuruoka, S. Mizutani, M. Tsujimoto, *Eur. J. Biochem.* **2001**, *268*, 3259–3266.
[7] B. Alescio-Lautier, V. Paban, B. Soumireu-Mourat, *Eur. J. Pharmacol.* **2000**, *405*, 63–72.
[8] M. G. Wallis, M. F. Lankford, S. R. Keller, *Am. J. Physiol. Endocrinol. Metab.* **2007**, *293*, E1092–E1102.
[9] J. J. Herbst, S. A. Ross, H. M. Scott, S. A. Bobin, N. J. Morris, G. E. Lienhard, S. R. Keller, *Am. J. Physiol.* **1997**, *272*, E600-E606.
[10] N. J. Bryant, R. Govers, D. E. James, *Nat. Rev. Mol. Cell Biol.* **2002**, *3*, 267–277.
[11] S. B. Waters, M. D'Auria, S. S. Martin, C. Nguyen, L. M. Kozma, K. L. Luskey, *J. Biol. Chem.* **1997**, *272*, 23323–23327.
[12] L. Saveanu, P. van Endert, *Front. Immunol.* **2012**, *3*, 1–13.
[13] E. Segura, A. L. Albiston, I. P. Wicks, S. Y. Chai, J. A. Villadangos, *Proc. Natl. Acad. Sci. USA* **2009**, *106*, 20377–20381.
[14] I. Evnouchidou, A. Papakyriakou, E. Stratikos, *Curr. Pharm. Des.* **2009**, *15*, 3656–3670.
[15] E. Stratikos, *Curr. Opin. Chem. Biol.* **2014**, *23*, 1–7.
[16] A. Lukaszuk, H. Demaegdt, D. Feytens, P. Vanderheyden, G. Vauquelin, D. Tourwé, *J. Med. Chem.* **2009**, *52*, 5612–5618.
[17] A. Nikolaou, I. Van Den Eynde, D. Tourwé, G. Vauquelin, G. Tóth, J. R. Mallareddy, M. Poglitsch, J. a Van Ginderachter, P. M. L. Vanderheyden, I. Van den Eynde, D. Tourwé, G. Vauquelin, G. Tóth, J. R. Mallareddy, M. Poglitsch, J. A. van Ginderochter, P. M. L. Vanderheyden, *Eur. J. Pharmacol.* **2013**, *702*, 93–102.
[18] A. Papakyriakou, E. Zervoudi, E. a Theodorakis, L. Saveanu, E. Stratikos, D. Vourloumis, *Bioorg. Med. Chem. Lett.* **2013**, *23*, 4832–4836.
[19] E. Zervoudi, E. Saridakis, J. R. Birtley, S. S. Seregin, E. Reeves, P. Kokkala, Y. A. Aldhamen, A. Amalfitano, I. M. Mavridis, E. James, D. Georgiadis, E. Stratikos, *Proc. Natl. Acad. Sci. USA* **2013**, *110*, 19890–19895.
[20] A. Papakyriakou, E. Zervoudi, S. Tsoukalidou, F.-X. Mauvais, G. Sfyroera, D. C. Mastellos, P. van Endert, E. A. Theodorakis, D. Vourloumis, E. Stratikos, *J. Med. Chem.* **2015**, *58*, 1524–1543.
[21] H. Andersson, H. Demaegdt, G. Vauquelin, G. Lindeberg, A. Karlén, M. Hallberg, *Bioorg. Med. Chem.* **2008**, *16*, 6924–6935.
[22] A. Axén, G. Lindeberg, H. Demaegdt, G. Vauquelin, A. Karlén, M. Hallberg, *J. Pept. Sci.* **2006**, *12*, 705–13.
[23] A. Axén, H. Andersson, G. Lindeberg, H. Rönnholm, J. Kortesmaa, H. Demaegdt, G. Vauquelin, A. Karlén, M. Hallberg, *J. Pept. Sci.* **2007**, *13*, 434–44.
[24] H. Andersson, H. Demaegdt, G. Vauquelin, G. Lindeberg, A. Karlén, M. Hallberg, M. Erdélyi, A. Hallberg, *J. Med. Chem.* **2010**, *53*, 8059–8071.
[25] H. Andersson, H. Demaegdt, A. Johnsson, G. Vauquelin, G. Lindeberg, M. Hallberg, M. Erdelyi, A. Karlen, A. Hallberg, *J. Med. Chem.* **2011**, *54*, 3779–3792.
[26] S. Diwakarla, E. Nylander, A. Gronbladh, S. R. Vanga, Y. S. Khan, H. Gutierrez-de-Teran, L. Ng, V. Pham, J. Savmarker, T. Lundback, A. Jenmalm-Jensen, H. Andersson, K. Engen, U. Rosenström, M. Larhed, J. Åqvist, S. Y. Chai, M. Hallberg, *Mol. Pharmacol.* **2016**, *89*, 413–424.

[27] A. L. Albiston, C. J. Morton, H. L. Ng, V. Pham, H. R. Yeatman, S. Ye, R. N. Fernando, D. De Bundel, D. B. Ascher, F. A. O. Mendelsohn, M. W. Parker, S. Y. Chai, *FASEB J.* **2008**, *22*, 4209–4217.
[28] B. Seyer, S. Diwakarla, P. Burns, A. Hallberg, A. Grönbladh, M. Hallberg, S. Y. Chai, *J. Neurochem.* **2019**, jnc.14880.
[29] S. J. Mountford, A. L. Albiston, W. N. Charman, L. Ng, J. K. Holien, M. W. Parker, J. A. Nicolazzo, P. E. Thompson, S. Y. Chai, *J. Med. Chem.* **2014**, *57*, 1368–1377.
[30] K. Engen, U. Rosenström, H. Axelsson, V. Konda, L. Dahllund, M. Otrocka, K. Sigmundsson, A. Nikolaou, G. Vauquelin, M. Hallberg, A. Jenmalm-Jensen, T. Lundbäck, M. Larhed, *Assay Drug Dev. Technol.* **2016**, *14*, 180–193.
[31] S. R. Borhade, U. Rosenström, J. Sävmarker, T. Lundbäck, A. Jenmalm-Jensen, K. Sigmundsson, H. Axelsson, F. Svensson, V. Konda, C. Sköld, M. Larhed, M. Hallberg, *ChemistryOpen* **2014**, *3*, 256–263.
[32] S. R. Vanga, J. Sävmarker, L. Ng, M. Larhed, M. Hallberg, J. Åqvist, A. Hallberg, S. Y. Chai, H. Gutiérrez-de-Terán, *ACS Omega* **2018**, *3*, 4509–4521.
[33] S. Diwakarla, E. Nylander, A. Grönbladh, S. R. Vanga, Y. S. Khan, H. Gutiérrez-de-Terán, J. Sävmarker, L. Ng, V. Pham, T. Lundbäck, A. Jenmalm-Jensen, R. Svensson, P. Artursson, S. Zelleroth, K. Engen, U. Rosenström, M. Larhed, J. Åqvist, S. Y. Chai, M. Hallberg, *ACS Chem. Neurosci.* **2016**, *7*, 1383–1392.
[34] X. Cheng, S. Vellalath, R. Goddard, B. List, *J. Am. Chem. Soc.* **2008**, *130*, 15786–15787.
[35] A. A. Mohammadi, M. Dabiri, H. Qaraat, *Tetrahedron* **2009**, *65*, 3804–3808.
[36] M. Dabiri, A. A. Mohammadi, H. Qaraat, *Monatsh. Chem.* **2008**, *140*, 401–404.
[37] Y. Hu, M.-M. Wang, H. Chen, D.-Q. Shi, *Tetrahedron* **2011**, *67*, 9342–9346.
[38] M. Narasimhulu, Y. R. Lee, *Tetrahedron* **2011**, *67*, 9627–9634.
[39] J. Zhang, J. Zhao, L. Wang, J. Liu, D. Ren, Y. Ma, *Tetrahedron* **2016**, *72*, 936–943.
[40] M. Larhed, A. Hallberg, *Drug Discovery Today* **2001**, *6*, 406–416.
[41] K. Engen, J. Sävmarker, U. Rosenström, J. Wannberg, T. Lundbäck, A. Jenmalm-Jensen, M. Larhed, *Org. Process Res. Dev.* **2014**, *18*, 1582–1588.
[42] A. Mpakali, E. Saridakis, K. Harlos, Y. Zhao, P. Kokkala, D. Georgiadis, P. Giastas, A. Papakyriakou, E. Stratikos, *J. Med. Chem.* **2017**, *60*, 2963–2972.
[43] S. Kortagere, S. Ekins, W. J. Welsh, *J. Mol. Graphics Modell.* **2008**, *27*, 170–177.
[44] F. Tholander, *PLoS One* **2012**, 7, e46764.
[45] S. J. Hermans, D. B. Ascher, N. C. Hancock, J. K. Holien, B. J. Michell, S. Yeen Chai, C. J. Morton, M. W. Parker, *Protein Sci.* **2015**, *24*, 190–199.
[46] R. A. Friesner, J. L. Banks, R. B. Murphy, T. A. Halgren, J. J. Klicic, D. T. Mainz, M. P. Repasky, E. H. Knoll, M. Shelley, J. K. Perry, D. E. Shaw, P. Francis, P. S. Shenkin, *J. Med. Chem.* **2004**, *47*, 1739–1749.
[47] R. A. Friesner, R. B. Murphy, M. P. Repasky, L. L. Frye, J. R. Greenwood, T. A. Halgren, P. C. Sanschagrin, D. T. Mainz, *J. Med. Chem.* **2006**, *49*, 6177–6196.
[48] J. Marelius, K. Kolmodin, I. Feierberg, J. Aqvist, *J. Mol. Graphics Modell.* **1998**, *16*, 213–225.
[49] W. L. Jorgensen, A. David S Maxwell, J. Tirado-Rives, *J. Am. Chem. Soc.* **1996**, *118*, 11225–11236.
[50] W. L. Jorgensen, J. Chandrasekhar, J. D. Madura, R. W. Impey, M. L. Klein, *J. Chem. Phys.* **1983**, *79*, 926–935.
[51] G. King, A. Warshel, *J. Chem. Phys.* **1989**, *91*, 3647–3661.
[52] H. Demaegdt, P. Vanderheyden, J.-P. De Backer, S. Mosselmans, H. Laeremans, M. T. Le, V. Kersemans, Y. Michotte, G. Vauquelin, *Biochem. Pharmacol.* **2004**, *68*, 885–892.
[53] J. Wernevik, F. Bergström, A. Novén, J. Hulthe, L. Fredlund, D. Addison, J. Holmgren, P.-E. Strömstedt, E. Rehnström, T. Lundbäck, *Submitted*.

Manuscript received: November 22, 2019
Revised manuscript received: January 23, 2020